

Rare Earth Elements abundance, fractionation, and anomalies in the sediments of the Cananéia-Iguape Estuarine-Lagoon Complex in Brazil

Vitor G. Chiozzini¹ , Deborah I. T. Fávoro² , Elisabete S. Braga¹ 

¹ Oceanographic Institute - University of São Paulo (Praça Oceanográfico, 191 - São Paulo - SP - 05508-120 Brazil).

² Nuclear and Energy Research Institute (Avenida Prof. Lineu Prestes, 2242 - Cidade Universitária, São Paulo - SP -05508-000 - Brazil).

* Corresponding author: vitor.chio@usp.br

ABSTRACT

The Cananéia-Iguape Estuarine-Lagoon Complex (CIELC) is an extremely productive coastal ecosystem. It encloses the Valo Grande channel, built 160 years ago, which introduces water from the Ribeira River directly into the estuarine system, contributing to important biogeochemical changes in the region. Many nutrients arrive at the estuary through this channel, as well as metals and other slightly soluble elements that become part of the sediments. This study aims to evaluate the processes that govern the distribution of rare earth elements (REE) in the sediments of the complex by using fractionation patterns, anomalies, and the geochemical signature of minerals to evaluate sources, natural levels, and the possible anthropogenic forcing to which CIELC is subjected. ΣREE^* ranged from 14.2 to 285 mg kg^{-1} and showed a distribution related to depositional/textural characteristics influenced by the regional and local lithological setting and a possible contamination. The REE/Al ratio indicated enrichment in the sea adjacent to the estuary and at stations in the Ribeira River and Valo Grande. While the Hf/Al ratio indicated natural enrichment related to the presence of heavy minerals in most of these stations, this ratio fails to justify enrichment at some stations in the northern part of the estuary and the Ribeira River. Fractionation patterns and anomalies allowed us to identify the main heavy minerals related to REE enrichment at CIELC. Cerium (Ce) anomalies showed a possible relation with biologically mediated Ce^{+3} to Ce^{+4} oxidation processes in the most productive areas of the estuary. Europium (Eu) anomalies were strongly associated with different mineral assemblies in several CIELC sectors. Abundance, fractionation patterns, and REE anomalies corroborate the categorization of CIELC sediments as part of a pristine system in its southern region and as subject to anthropogenic influences in its northern area.

Descriptors: REE Geochemistry, Estuarine RAMSAR Area, Trace Metals, Biogeochemistry, Phosphogypsum

INTRODUCTION

Rare earth elements (REE) configure a group of 15 elements that range from lanthanum (La; the

lightest) to lutetium (Lu; the heaviest). According to Moeller (1985), the chemical properties of these elements are systematically influenced by differences in their electronic structures, which involve electrons in internal orbitals, whereas external orbitals are involved in chemical bonds with other atoms. The increase in the charge of the atomic nuclei throughout the group contracts their atomic orbitals, slightly decreasing the ionic

Submitted: 28-jun-2022

Approved: 09-jul-2023

Editor: Rubens Lopes

Associate Editor: Juliana Azevedo



© 2023 The authors. This is an open access article distributed under the terms of the Creative Commons license.

radius of these elements as their atomic numbers increases, an effect known as “lanthanide contraction”. The relatively regular variation in the ionic radius of REE is of enormous importance to their chemical properties; each element within this group has remarkably similar characteristics to its neighbors but significantly different characteristics to elements with distant atomic numbers (Henderson, 1984; Moeller, 1985). Thus, REE are typically classified into subgroups. Members of the lanthanum series with low atomic numbers are called light rare earth elements (LREE); those with the highest atomic numbers are called heavy rare earth elements (HREE); and the intermediate members, from samarium (Sm) to terbium (Tb), are known as intermediate/medium rare earth elements (MREE).

All REE are trivalent in natural environments, except for europium (Eu – Eu^{+2} and Eu^{+3}) and cerium (Ce – Ce^{+3} and Ce^{+4}). Eu^{+2} suffers a lower power of attraction from its nucleus over its electronic layers due to its additional electron, causing it to have a greater ionic radius. The same happens with Ce^{+4} . As it has one less electron than its trivalent speciation, its nucleus more greatly attracts its electronic layers, resulting in a smaller ionic radius. The oxidation states of these two elements alter their reactivity characteristics, which can change their relative environmental abundances in comparison to their trivalent neighbors. This change in abundance can be identified as an anomaly. If the abundance of Ce or Eu is slightly higher than expected compared to its trivalent neighbors, it is called positive. On the other hand, if the observed abundance is less than expected, it is called negative.

REE have important geochemical properties that enable them to be used as indicators of several geochemical processes in natural environments. Geologically, these elements are considered incompatible: They are mainly incorporated into the crystalline net of common minerals by replacing elements with similar ionic radius. Thus, the main causes of the variation in the distribution of REE on rocks refer to their incorporation to mineral structures and the paragenetic conditions of mineral formation (Henderson, 1984). Although some authors have shown that chemical weathering

can mobilize REE (Balashov et al., 1964; Burkov and Podporina, 1967; Nesbitt, 1979; Leroy and Turpin, 1988; Rolland et al., 2003; Maulana et al., 2014; Vinnarasi et al., 2020), these elements are considered to have low mobility and their content in sedimentary rocks naturally reflects the mineral content of their source rocks and the processes which formed the minerals incorporated into such sources (McLennan, 1989; Yang et al., 2002; Armstrong-Altrin et al., 2012).

These characteristics make REE good tracers of the sources of terrestrial material in sediments and a powerful tool to indicate sedimentary provenance and depositional processes in estuarine and coastal systems (e.g., Chaillou et al., 2006; Marmolejo-Rodríguez et al., 2007; Prego et al., 2009; Liu et al., 2013; Um et al., 2013; Fiket et al., 2017; Rao et al., 2017; Wu et al., 2019; Kechiched et al., 2020; Slukovskii et al., 2022), scavenging processes and the chemical weathering of drainage basins (e.g., Byrne and Kim, 1990; Bau, 1999; Haley et al., 2004; Bau and Koschinsky, 2009; Yusoff et al., 2013; Su et al., 2017), and anthropogenic inputs on sediments (e.g., Elbaz-Poulichet and Dupuy, 1999; Borrego et al., 2004, 2012; Oliveira et al., 2007; Hannigan et al., 2010; Shynu et al., 2011; Tranchida et al., 2011; Pérez-López et al., 2016; Elias et al., 2019; Godwyn-Paulson et al., 2022). According to Schäfer et al. (2016), these elements are currently considered as emerging inorganic contaminants, having an increasing relevance and demand as critical elements for the construction of technological products. Moreover, REE can accumulate on ore beneficiation by-products, phosphate rock mining, among others, and be carried to rivers.

Estuarine systems are often the destination for compounds originated during continental weathering and as a result of anthropogenic action. These environments undergo large and rapid variations in their physicochemical gradients and local conditions, such as advective transport, changes in redox conditions, mixing of fresh and saline waters, etc., receiving sediments from both fluvial and marine sources and being able to retain trace metals and diversified organic compounds. The distribution of REE and other elements of

environmental concern in estuarine sediments are especially useful for assessing provenance and environmental quality, especially on transport and continent/ocean interface processes. Thus, the main focus of this study was to evaluate REE abundance, fractionation and anomalies; determine the major processes and factors controlling the concentration of these elements in the sediments of the Cananéia-Iguape Estuary-Lagoon Complex (CIELC), an estuary recognized as an Atlantic Forest Biosphere Reserve by the United Nations Educational, Scientific and Cultural Organization (UNESCO), and its connections to the sea; understand natural distribution patterns, sources, and the influence of the local geology; and check possible regions subject to deposits of contaminated sediments. The functions, effects, and environmental fates of these elements have received increasing attention, therefore its distribution is of profound interest to coastal and estuarine science.

METHODS

STUDY AREA

CIELC covers a large portion of the southern coast of São Paulo State, Brazil, is more than 90 km long, and comprises four islands surrounded by estuarine and tidal channels and coastal lagoons. Its northern part has an artificial channel that links the Ribeira River to its estuarine waters (Figure 1a).

CIELC has three connections to the adjacent ocean: one to the north, the Icapara bar, and two others to the south, the Cananeia and Ararapira bars. The most important drainage basin that supplies the system with fresh water has approximately 23,350 Km² and converges mainly to the Ribeira River (Almeida, 1976). The outflow in its lower course varies from about 100 to more than 1500 m³ s⁻¹. This variation is strongly controlled by the climatic regime (Tessler and Furtado, 1983; Bérnago, 2000).

At Iguape, in northern CIELC, part of the flow of the Ribeira River was diverted after the construction of the artificial Valo Grande channel from 1828 to 1852. It was built to facilitate transportation of goods between the Ribeira River and the estuary, in which lied the main local export

harbor. With a length of less than 4 km, it originally was 4.4 m wide and 2.0 m deep. Transport of terrestrial material from its bed and margins has widened the channel, changing the ecological and physic-chemical characteristics of northern CIELC. Nowadays, the artificial channel of the Valo Grande is more than 250 m wide with a maximum depth of 12 m. About 60% of the discharge of the Ribeira River is diverted directly into CIELC by Valo Grande (Ribeira de Iguape and South Coast Hydrographic Basin Committee, 2008), introducing a large amount of fresh water into CIELC, excavating and carrying a large amount of suspended material and sediments (Tessler and Furtado, 1983) and contributing to increasing the introduction of nutrients and contaminants into CIELC as a whole (Braga and Chiozzini, 2012).

The artificial Valo Grande channel is the main human environmental impact in CIELC. The Ribeira River drainage basin holds some of the largest ore deposits in São Paulo State. Mining activities began in the region during the gold rush in the 16th century. Later, mining activities extracted and industrially processed lead, which directly impacted the local water bodies in the 20th century (Guimarães and Sígolo, 2008; Mahiques et al., 2013; Tramonte et al., 2018). Mining phosphate rock for fertilizers has taken place since 1938 in the Ribeira River basin, which has also been shown to be an impact vector for the CIELC. Some authors have related the high levels of phosphate entering the estuary through the Valo Grande to the mining of phosphate rocks, which mainly takes place in Cajati (CETESB, 2013).

Water circulation is mainly driven by the action of tidal waves (Miyao et al., 1986). The freshwater contribution of rivers, mainly through the Valo Grande, also plays an important role in the circulation of CIELC.

Regarding its geological background, the Ribeira River basin has great lithological-structural complexity (Figure 1b). The Ribeira River basin lies in a region comprising three major geological domains. According to Ross (2002), its upper lands shows rocks predominantly composed of granite types, quartzites, granitic gneisses, phyllites, mica schists, calcareous, and dolomite. Ridges rise from this level sustained by granites, quartzites or even

by more erosion-resistant calcareous tops from 1050 to 1150 m heights. From this area, the Ribeira River basin progressively loses altitude, defining reliefs in the form of hills that are steeply carved in less weathering-resistant metasedimentary rocks - especially phyllites, mica schists, and limestone, which also relate to local mineral deposits (Souza et al., 1996). Unconsolidated marine sandy sediments prevail in the coastal lowlands and the inner plains have recent river deposits and alluvial and colluvium-alluvial species selected from Pleistocene formations (Almeida, 1976; Ross, 2002). In the coastal plain, a pre-Cambrian crystalline basement outcrop occurs to the north, near the municipality of Iguape, whereas, in the center and to the south, the Cardoso Island consists of metamorphic rocks such as phyllites, mica schists, and gneisses. Mesozoic intrusive alkaline rocks appear near the urbanized region of Cananéia.

The Ribeira River basin comprises about half of all the native vegetation of São Paulo State and is one of the largest preserved areas of the Atlantic Rainforest (Veloso et al., 1991), showing the native Atlantic Forest biome, dense ombrophilous vegetation, mixed ombrophilous forest, and altitude fields. The prevailing vegetation in the CIELC plain consists of well-structured mangroves, marshes, and the *restinga* (SUDELPA, 1987; Cunha-Lignon, 2001).

The southern portion of the draining basin (in the Cananéia region) consists of a small hydrographic system, which drains mainly into the internal portion of the Trapandé Bay. According to Bérgho (2000), annual discharge varies from 5.8 to 100 m³ s⁻¹. Tidal effects are more efficient in this sector, constantly renewing the local water. The absence of industry occupation and the low population (working in fishing and tourism) contribute to a lower anthropic impact in this sector of the system.

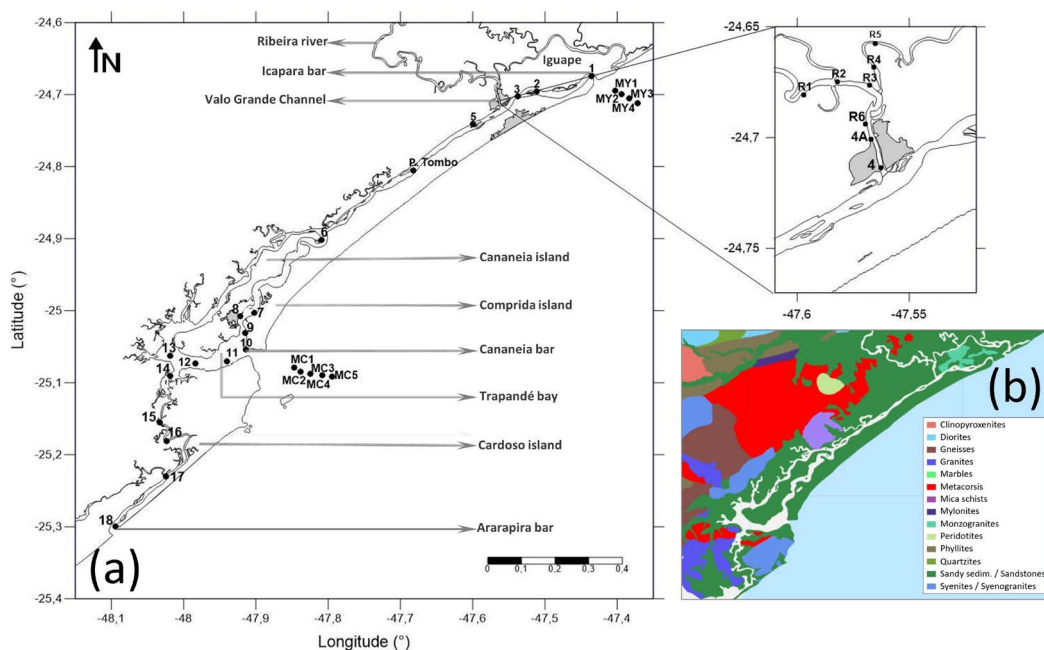


Figure 1. Location of the CIELC (São Paulo, Brazil). Sediment sampling points (a) and a simplified map of the lithology of CIELC (b).

SAMPLING

Surface sediment samples were collected at 34 locations in CIELC (Figure 1a). Its two regions (north and south) were subdivided into six sectors, three of which were in northern CIELC and three in southern CIELC.

Northern CIELC sectors were divided as follows: (i) Ribeira River, comprising stations R1, R2, R3, R4, R5, and R6; (ii) the sea adjacent to northern CIELC, comprising stations MY1, MY2, MY3, and MY4; and (iii) Pequeno sea/Iguape, comprising stations 1, 2, 3, 4, 4A, 5, and P. Tombo. Southern

sectors were divided thus: (iv) Cananéia sea and Trapandé Bay, including stations 6 to 12; (v) the Ararapira channel, including stations 13 to 18; and (vi) the sea adjacent to southern CIELC, comprising stations MC1, MC2, MC3, MC4, and MC5.

Surface sediments were sampled using a stainless-steel van Veen grab with an area of 0.05 m², collecting aliquots of about 3 cm of the surface layer of the sediment in the center of the device. Approximately 30 g of each sample were stored in polycarbonate vials with polyethylene caps, which had previously been washed with a solution of 2 mol L⁻¹ HCl, rinsed with ultrapure water, and dried at room temperature. The tubes containing the samples were frozen at -20°C and lyophilized after a few days. Sediments were then disaggregated using an agate mortar and pestle, homogenized, reset in their original vials, and stored in a desiccator containing silica gel, from which they were only removed for subsequent determinations.

ANALYTICAL PROCEDURES AND QUALITY CONTROL

The organic matter and biotrititic carbonate in the sediments were evaluated using gravimetry after 5.0 g of the samples were treated with 1.0 mol L⁻¹ H₂O₂ at 60°C and 1.0 mol L⁻¹ HCl, respectively. Grain size was analyzed using the sediments resulting from the elimination of organic matter and biotrititic carbonate. These were then dispersed in 2.0 mL of a 1% sodium hexa-meta phosphate solution and analyzed by low-angle laser light scattering (LALLS) using a Malvern® Mastersizer 2000 analyzer.

REE (La, Ce, Nd, Sm, Eu, Gd, Tb, Tm, Yb, and Lu) and Hf, Th, Zr content was determined by instrumental neutron activation analysis (INAA) at the Nuclear and Energy Research Institute (IPEN/CNEN). Briefly, 200-mg sample aliquots were weighed and packed in cleaned polyethylene capsules (HNO₃ at 2.0 mol L⁻¹ and ultrapure water). The same procedure was used to prepare the three reference materials: Soil-5 (IAEA), BEN Basalt (CNRS), and BRP-1 (CRPM and USGS). Samples and reference materials were then alternately placed in a cylindrical aluminum cap, which was sealed and sent to the research reactor IEA-R1, in which they were subjected to a neutron flux of 1

to 5 × 10¹² n cm⁻² s⁻¹ for eight hours. After cooling, the counting rate was obtained for the samples and reference materials by gamma spectrometry using a semiconductor (hyperpure Ge) detector connected to a CANBERRA® 8192 multichannel system (model GMX2020) and associated electronics. Expanded uncertainties were calculated by a coverage factor (k=2), the combined uncertainties from counting statistics (major contribution), and uncertainties of the certified material analysis. Our methodology was validated by reference materials analysis.

To verify methodological accuracy, two analyzed reference materials were used as standards to calculate the concentration of each element determined in the third reference material. Results were compared to the certified values and the relative error (RE) and the relative standard deviation (RSD) were calculated (Table S1, Supplementary Material). Good agreement between the obtained and certified concentrations was achieved for all elements.

Aluminum (Al) content was determined by laser-induced breakdown spectrometry (LIBS) using the comparative technique at the Institute of Chemistry at the University of São Paulo. In total, 450 mg of each sample and certified reference material were precisely added to 50.0 mg of pure SPEX® Sample Prep Aid (binder). The sample and binder were macerated with an agate mortar and pestle to form a homogeneous mixture, transferred to a set of molds, and compacted in a SPEX® 3635 X-PRESS hydraulic press at a pressure of 10-tonne cm⁻² for 10 minutes to form a uniform surface tablet. Overall, six certified reference materials were used to construct the analytical curve: BEN Basalt (CNRS), Soil-5 (IAEA), IAEA 405 (IAEA), BRP-1 (CRPM/USGS), marine sediment MESS-3 (NRCC), and estuarine sediment SRM-1646a (NIST). The samples and reference materials/standards were analyzed using Applied Spectra® J200 TANDEM equipment in an argon atmosphere. The values for each certified reference material were calculated using the other five reference materials as standard. Obtained results agreed to the certified values (Table S2), showing REs below 6.1%.

All determinations were performed in duplicates. RSD among replicates averaged 3%

and never exceeded 6.7% in any sample for all determined parameters.

DATA TREATMENT

REE NORMALIZATION BY VALUES OF THE UPPER CONTINENTAL CRUST (UCC)

Normalization was undertaken using the UCC as the geological standard, with values following Wedepohl (1995), to eliminate the Oddo–Harkins effect caused by variation in natural abundance throughout the lanthanum series and to facilitate the identification of fractionation patterns between the REE.

The abbreviation $[REE]_{UCC}$ will be used to represent the normalized value of a given REE by the values suggested for the UCC. Values of $[REE]_{UCC}$ greater than 1.00 indicate enrichment of the REE, and values lower than 1.00 indicate depletion in relation to the UCC values.

Σ REE AND NORMALIZED La/Sm, La/Yb, Sm/Yb, AND Sm/Nd RATIOS

Σ REE was determined by adding La, Ce, Nd, Sm, Eu, Gd, Tb, Tm, Yb, and Lu values, in mg kg⁻¹. The used analytical method determines most of REE and the Σ REE* will be referred as the sum of determined REE in this study. Values of $[\Sigma$ REE*]_{UCC} were also determined by the sum of the values of each REE* in the samples divided by the sum of the values suggested for the UCC for that REE*.

$$[\Sigma REE^*]_{UCC} = \frac{\Sigma REE^*}{\Sigma REE^*_{UCC}}$$

Normalized La/Sm, La/Yb, and Sm/Yb ratios were calculated according to the following equations:

$$[La/Sm]_{UCC} = \frac{[La]_{UCC}}{[Sm]_{UCC}}$$

$$[La/Yb]_{UCC} = \frac{[La]_{UCC}}{[Yb]_{UCC}}$$

$$[Sm/Yb]_{UCC} = \frac{[Sm]_{UCC}}{[Yb]_{UCC}}$$

$$[Sm/Nd]_{UCC} = \frac{[Sm]_{UCC}}{[Nd]_{UCC}}$$

CE AND EU ANOMALIES

Ce and Eu anomalies were calculated according to equations proposed by Taylor and McLennan (1985):

$$[Ce/Ce^*]_{UCC} = \frac{3[Ce]_{UCC}}{2[La]_{UCC} + [Nd]_{UCC}}$$

$$[Eu/Eu^*]_{UCC} = \frac{[Eu]_{UCC}}{\sqrt{[Sm]_{UCC} \times [Gd]_{UCC}}}$$

In which:

Ce/Ce^* – Ce anomaly (obtained Ce/predicted Ce by the neighbouring La and Nd);

Eu/Eu^* – Eu anomaly (obtained Eu/predicted Eu by the neighbouring Sm and Gd);

STATISTICS

Spatial distribution maps were created using Surfer 13[®]. Statistical treatments—including distribution tests, correlation matrices, and bivariate scatter diagrams—were created using Statistica 13[®].

RESULTS AND DISCUSSION

GRANULOMETRY AND TEXTURAL COMPOSITION

We observed a predominance of sandy sediments in practically all the CIELC, including in the stations in the Ribeira River and in the sea adjacent to the Icapara and Cananéia bars (Figure 2).

Table S3 shows Folk and Ward's (1957) statistical parameters. Average grain diameter varied from 1.48 to 6.98 ϕ .

Ribeira River samples predominantly consisted of fine and medium sands, with silt and clay contents below 10%. Only R6, located in a river basin before Valo Grande and under low hydrodynamic energy showed a great silt and clay content (64.2%).

Pequeno sea sediments also showed a dominance of fine and medium sands, except for station 2 (which had a considerable silt and clay content – 45.5%) and the P. Tombo station (99.9%). The latter lies in an area with low hydrodynamic energy, a suitable region for fine sediment deposition. Tessler and Souza (1998) indicate that an accumulation of fine sediments occurs in areas in which southern and northern tides converge (P. Tombo). We observed that the predominance of high hydrodynamic conditions and the continuous erosion processes of the margins along Valo Grande precluded fine sediment retention. We hypothesize that a large part of the sediment transported across Valo Grande will be deposited in P. Tombo due to its low energy.

in stations with little or no material < 63 μm , as in stations R3, 1, 5, and 10. We observed the highest values in station R6, P. Tombo, and 13, whose fine fractions were more relevant.

Biotrititic carbonate amounts (Figure 3c) varied widely. Considering the entire system, 65% of samples had levels above 2%. We found the lowest values at stations R1 and R3 (in the Ribeira River; 0.10 and 0.15%, respectively) and the highest values at stations 15 and 16 (in the central part of the Ararapira channel; 11.0 and 10.1%, respectively); in which we observed submerged *sambaquis* (prehistoric mounds containing the shells of marine mollusks made by Indigenous people a few thousand years ago, when the sea level was lower). In general, the inner northern CIELC had the

lowest levels of biotrititic carbonate, except in station R6 (5.16%). We considered all samples as lithoclastic, according to the classification proposed by Larssoneur et al. (1982).

The textural composition of the superficial sediments along CIELC reflects hydrodynamics and the important influences of tides, erosion, transport, and the deposition of natural and anthropic materials, which enter the estuary from the Ribeira River after traveling through Valo Grande. Their interaction with marine waters results in an important inflow of fine suspended sediments, which are deposited in specific regions (especially in the northern region, in the northeastern vicinity of P. Tombo), mainly transported southward during the rainy season and exported from the complex to the adjacent sea.

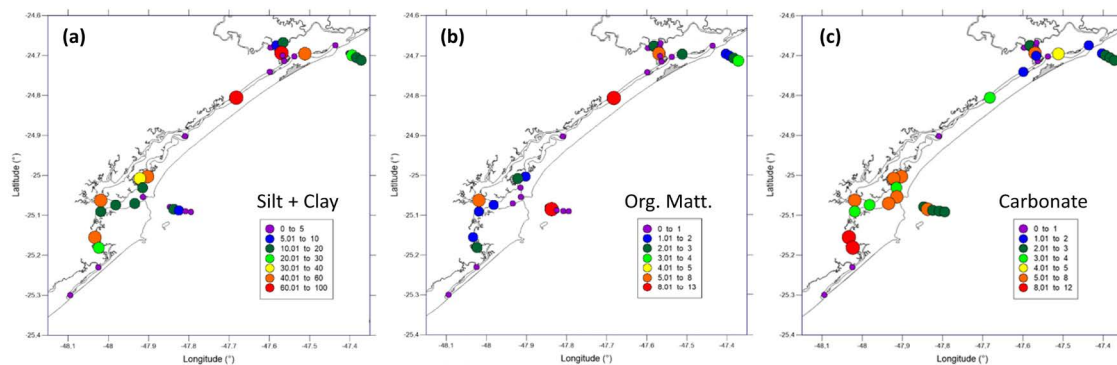


Figure 3. Distribution of silt and clay (a), organic matter (b), and carbonate (c) contents in the surface sediment of CIELC and the sea adjacent to the Cananéia and Icapara bars.

REE* AND ELEMENTAL BALANCES

The geochemical composition of surface sediments reflects the composition of the original matrix and indicates the action of deposition, resuspension, dissolution, precipitation, hydrodynamic, pollution, and several other environmental processes associated with the system. In our case, some differences between CIELC sectors have already been identified thanks to granulometric analysis and the examination of the organic matter and carbonate content of these sediments. This segment of our study will highlight some environmental aspects, considering REE* (La, Ce, Nd, Sm, Eu, Gd, Tb, Tm, Yb, and Lu) and their associations with, Hf, Th, Al and Zr. Table S4 shows the individual concentrations of each of these elements throughout CIELC.

Al concentrations ranged from 1.23 to 8.02%, with the lowest value at station 18 and the highest value at station P. Tombo. Zr concentrations ranged from 31 to 924 mg kg^{-1} . We found the highest concentrations of this element at sea stations adjacent to the bars, both in northern and southern CIELC and at stations R1 and 4A and the lowest values at stations 18 (31 mg kg^{-1}), 4 (36 mg kg^{-1}), and 10 (37 mg kg^{-1}). Hf levels ranged from 1.1 to 45.0 mg kg^{-1} with a remarkably similar distribution to that of Zr. Th concentrations showed their highest values at sea stations MY3 and MY2 (16.2 and 16.1 mg kg^{-1} , respectively) and their lowest values at stations 18 and 17 (0.67 and 1.19 mg kg^{-1} , respectively).

Total REE* concentrations (ΣREE^*) in CIELC surface sediments varied widely across sectors,

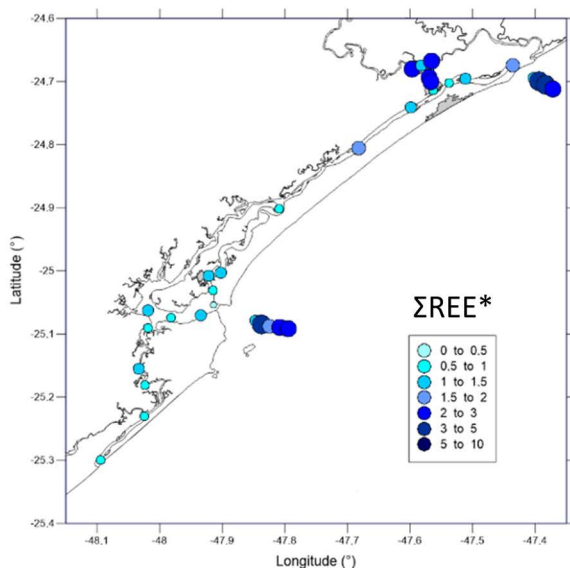
averaging 93.9 mg kg^{-1} . The stations with the highest values of this parameter were P. Tombo (285 mg kg^{-1}), R6 (272 mg kg^{-1}), MY3 (226 mg kg^{-1}), and MC2 (225 mg kg^{-1}). We observed the lowest values of ΣREE^* in stations 10 and 18 (14.2 and 14.3 mg kg^{-1} , respectively); whose silt and clay fractions were insignificant.

REE/Al ratios generally serve as a proxy for the possible enrichment of REE in sediments accumulated on continental margins (Calvert and Pedersen, 2007). We calculated Al-normalized REE for CIELC samples as the normalized double ratio based on samples and the values Wedepohl (1995) proposed for UCC as a geological standard.

$$[\text{REE}/\text{Al}]_{\text{UCC}} = \frac{\left(\frac{[\text{Ce}]}{[\text{En}]}\right)_{\text{sample}}}{\left(\frac{[\text{E}]}{[\text{En}]}\right)_{\text{UCC}}}$$

In which E_i is the concentration of the element of interest (REE* in this case) and E_n is the concentration of the normalizing element (Al).

Figure 4 showed the $[\text{REE}/\text{Al}]_{\text{UCC}}$ of ΣREE^* along CIELC (see to Figure S1 for the $[\text{REE}/\text{Al}]_{\text{UCC}}$ distribution of each REE*). $[\text{REE}/\text{Al}]_{\text{UCC}}$ mainly values show ΣREE^* enrichment (> 1.00) in adjacent sea stations, especially at MC2 (3.39), MY2 (3.19), MY3 (3.09), MY4 (2.25), MC5 (2.25), and MC4 (2.05); in the Ribeira stations, namely R4 (2.60), R6 (2.40), R1 (2.19), and 4A (2.16); and at the P. Tombo station (1.57). At the R6 and P. Tombo stations, enrichment levels were greater for LREE* and MREE* than for HREE*, whereas in the Ribeira River and adjacent sea stations, $[\text{REE}/\text{Al}]_{\text{UCC}}$ exceeded those of HREE*. Eu stands out as the only REE* with the highest $[\text{REE}/\text{Al}]_{\text{UCC}}$ value at a station inside the estuary (R6).



Summary of EF values					
	min.	at station		max	at station
ΣREE^*	0.48	(10)	to	3.39	(MC2)
La	0.45	(10)	to	3.50	(MC2)
Ce	0.41	(10)	to	3.27	(MC2)
Nd	0.48	(6)	to	3.90	(MY3)
Sm	0.48	(10)	to	3.51	(MC2)
Eu	0.55	(17)	to	2.68	(R6)
Gd	0.39	(10)	to	3.61	(MY2)
Tb	0.23	(10)	to	3.24	(MC2)
Tm	0.36	(7)	to	3.63	(MC2)
Yb	0.52	(6)	to	3.53	(MC2)
Lu	0.41	(10)	to	3.84	(MC2)

Figure 4. Distribution of $[\text{REE}/\text{Al}]_{\text{UCC}}$ values calculated using UCC concentrations of ΣREE^* in the surface sediments obtained at CIELC and the adjacent sea, summary of $[\text{REE}/\text{Al}]_{\text{UCC}}$ intervals obtained for each REE*, and the respective stations in which we observed such values.

Al-normalized elemental values from 2 to 5 can indicate moderate contamination. Although the internal region of estuaries show an intense deposition of sediments from continental weathering and anthropogenic action, we unexpectedly found the highest $[\text{REE}/\text{Al}]_{\text{UCC}}$ values at sea stations adjacent to northern and southern CIELC.

We used Spearman's correlation coefficient matrix (Table S5) to verify the degree of association between REE and other variables.

Al, which has the best correlation for silt and clay fractions ($r=0.91$), showed significant and positive correlation coefficients with ΣREE^* and each REE*: La ($r=0.80$), Ce ($r=0.82$), Nd ($r=0.78$), Sm

($r=0.84$), Eu ($r=0.92$), Gd($r=0.84$), Tb ($r=0.82$), Tm ($r=0.68$), Yb ($r=0.71$), and Lu ($r=0.67$). We found a clear trend of higher correlation coefficients of Al with MREE* and LREE* than with HREE*, with its highest correlation to Eu.

Zr showed significant REE* positive correlations: La ($r=0.81$), Ce ($r=0.78$), Nd ($r=0.80$), Sm ($r=0.80$), Eu ($r=0.67$), Gd ($r=0.79$), Tb ($r=0.79$), Tm ($r=0.79$), Yb ($r=0.83$), and Lu ($r=0.83$) and for the elements Hf ($r=0.89$) and Th ($r=0.83$). We found the lowest elemental correlation for Zr to Al ($r=0.50$). Antagonistic to the Al trend, Zr shows a tendency of higher correlations for HREE* than to LREE* and MREE* and the lowest correlation with Eu among REE*.

Hf showed a positive and significant correlation coefficient with REE* and the element Th ($r=0.77$). Regarding REE*, the best Hf associations also occurred for the HREEs Lu ($r=0.83$) and Yb ($r=0.79$), whereas we found the lowest correlation coefficient with Eu ($r=0.55$). Σ REE* showed a correlation coefficient of $r=0.71$ with Hf.

Considering Σ REE* and the other analyzed non-REE, it best correlated with Th ($r=0.98$).

Zr and Al showed significant correlations with Σ REE* ($r=0.80$ and 0.81 , respectively) but a weak correlation between themselves, indicating that the main distribution of these elements is subject to different processes. According to Humphris (1984), the chemistry governing the distribution of REE is a complex interaction between primary and secondary processes and no simple rule control their transportation in their different degrees of metamorphism. Since REE have a strong tendency to adsorb and co-precipitate in Fe and Mn oxyhydroxides and argillominerals (Elderfield et al., 1990), most REE in sediments may be within detrital clay and silt particles and in heavy mineral grains, such as ilmenite, monazite, and zirconite (Rasmussen et al., 1998), which have naturally high REE contents.

We built a matrix of correlation coefficients between the analyzed elements and each granulometric fraction considering data analyzed by laser diffractometry (Table S6). Among the evaluated elements, Al and Eu showed the highest correlation coefficients with all fine granulometric fractions, the best of which with medium silt ($r=0.93$

and 0.88 , respectively). For the other REE* and Th, we found the highest correlation coefficients with the sub-sandy coarse silt fraction, with a clear downward trend in correlation values throughout the series. Zr and Hf only showed weak positive correlations with the granulometric very fine sand fraction. The only REE* that showed a significant correlation coefficient with the very fine sand fraction were the HREE Tm, Yb, and Lu.

To assist our interpretation of results in view of the complexity of the studied sediments, we built scatter diagrams using the findings for silt and clay, Al, Hf, Zr, Th, and Σ REE* (Figure 5).

While Al fulfilled the requirement to normalize the sediments and minimize the effects of granulometric variation (Figure 5 a), it shows no linearity in the diagrams with Hf (Figure 5 b) and Zr (Figure 5 c). Despite their lack of linearity, these two elements show a similar scattering with Al, in which stations MC2, MY3, MY2, MC3, MC5 and 4A stood out for their high Zr and Hf values. The diagrams for Th with Al (Figure 5d), Σ REE* with silt and clay (Figure 5e), and Σ REE* with Al (Figure 5f) show very similar dispersions. The stations with high concentrations of Zr and Hf (MC2, MC3, MC5, MY2, MY3, MY4, and 4A) also stood out for their high levels of Th and REE*. However, the R6 station contains low levels of Zr and Hf and lies above the predicted Σ REE* levels in the regression line in these three cases. Plotting Σ REE* with Hf (Figure 5g) and Zr (Figure 5h) shows that station dispersions are remarkably similar in the diagram, with REE enrichment at R6 and P. Tombo, when compared to the low values of Hf and Zr. Th, an element with geochemical characteristics very similar to REE, showed an excellent linearity in its diagram with such elements (Figure 5i), indicating that the same processes and mineral sources probably act in the distribution of these elements. However, we found different results for the R6 and P. Tombo stations as REE exceeded the value predicted by the regression line, whereas MY2 showed a value slightly below that estimated by linear regression. The enrichment of Th in relation to Σ REE*, as evinced in station MY2, may suggest the differentiated presence of heavy minerals. Specific mineralogical studies are required to verify the degree of influence of a possible

difference in mineralogical composition between these sectors and/or a possible REE desorption at salinities close to 10 with subsequent readsorption in salinities above 15, as described by Lawrence

and Kamber (2006). Such process must occur in the northern region in a more pronounced way as it is more susceptible to sudden changes in salinity levels than the southern sector.

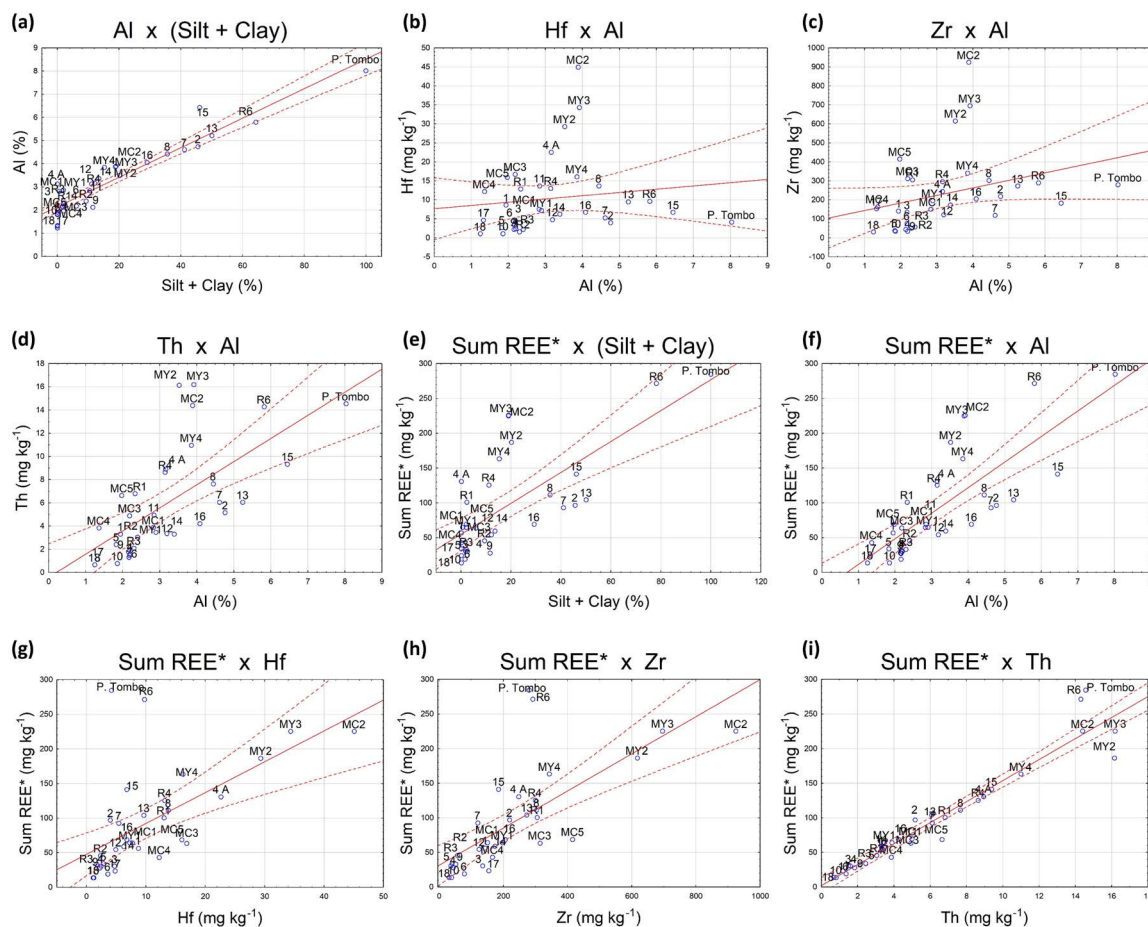


Figure 5. Scatter diagrams of Al with the silt and clay fraction (a), Hf and Al (b), Zr with Al (c), Th with Al (d), Σ REE* with silt and clay (e), Σ REE* with Al (f), Σ REE* with Hf (g), Σ REE* with Zr (h), and Σ REE* with Th (i) in CIELC and adjacent sea surface sediments.

A comparative study of correlations and scatter diagrams shows that CIELC REE values are mainly driven by the Al-enriched distribution of secondary minerals and the presence of different mineral assemblies—especially heavy minerals since Zr and Hf indicate the presence of such minerals.

According to Schropp and Windom (1988), the interpretation of metal values in sediments is hampered by the fact that the absolute concentration is subject to a wide variety of factors, including sediment mineralogy, granulometry, carbonate and organic matter content, and factors

such as anthropogenic enrichment. Therefore, it is difficult to distinguish the extent to which natural factors, as opposed to human led, caused the observed concentrations (Kalis et al., 2003).

Heavy minerals may have a primary origin in a wide range of rocks, especially in igneous formations such as granitic pegmatites and syenites, and metamorphic environments, such as shale and gneisses, which can be used to trace sediment origin and indicate sedimentary dynamics. As mentioned (Figure 1b), the Ribeira River basin has all rock formations above as

heavy mineral suppliers. Heavy minerals such as ilmenite (FeTiO_3), zirconite (ZrSiO_4), rutile (TiO_2), hematite (Fe_2O_3), magnetite (Fe_3O_4), and monazite ($\text{LREE, Th}\text{PO}_4$), among others, indicate high energy depositional conditions (Dellwig et al., 2000; Hinrichs et al., 2002; Buynevich et al., 2004), resulting in the enrichment of Zr, Hf, Titanium (Ti), and Fe in sediments.

To verify the possible enrichment of heavy minerals in sediments, many authors use the Zr/Al ratio. The higher the Zr/Al values are, the higher the enrichment of heavy minerals in samples (Kolditz et al., 2012). The use of such ratio requires caution as values are low for both low hydrodynamic regions and very high energy environments, without $< 63\text{-}\mu\text{m}$ particle deposition.

This study used the Hf/Al ratio instead of the traditional Zr/Al ratio. Given the geochemical similarity and the mineralogical affinity between Hf and Zr—and considering the greater precision and accuracy of Hf than Zr in INAA analysis—the Hf/Al ratio is more accurate and adequate than the Zr/Al ratio in this case (Table S1). Hf/Al ratios for the surface sediment in the studied area showed values from 0.5×10^{-3} to 11.6×10^{-3} . We found the highest values in stations MC2 and MC4 (9.1×10^{-3}), MY3 (8.8×10^{-3}), MY2 (8.4×10^{-3}), MC3 (7.7×10^{-3}), 4A (7.2×10^{-3}), and R1 (5.6×10^{-3}). The other stations had $< 4.00 \times 10^{-3}$ Hf/Al ratios. We observed the lowest values for this parameter at P. Tombo and 10 (0.6×10^{-3}), R3 (0.7×10^{-3}), 18 (0.9×10^{-3}), R2 (1.0×10^{-3}), 4 (1.1×10^{-3}), 7 (1.2×10^{-3}), 12 (1.5×10^{-3}), 5 (1.5×10^{-3}), 6 (1.6×10^{-3}), and R6 (1.7×10^{-3}). These stations have very different depositional conditions, with R2, R3, 4, 5, 6, 10, and 18 under strong hydrodynamic conditions (in which we found no evident deposition of fine sediments) and stations P. Tombo, R6, 7, 12, and 13 under low to moderate hydrodynamic conditions.

Stations with high Hf/Al ratios coincide with those with the highest REE* enrichment. These stations lied in the sea adjacent to the northern and southern bars of CIELC and at stations R1 and 4A. However, the R6 and P. Tombo stations, also enriched in REE, showed no Hf/Al values to justify their high levels of these elements.

UCC-NORMALIZED REE PATTERNS AND FRACTIONATION

Normalized REE* values (Table S7) show a general depletion pattern (< 1.00) in relation to the suggested values for the UCC. Exceptions to this pattern occurred at stations R6, MY2, MY3, MY4, and P. Tombo in northern CIELC and at stations 15 and MC2 in southern CIELC (Figure 6).

Table S7 shows the $[\text{La}/\text{Sm}]_{\text{UCC}}$, $[\text{La}/\text{Yb}]_{\text{UCC}}$, and $[\text{Sm}/\text{Yb}]_{\text{UCC}}$ ratios, tools to measure the individual relative fractionation between the REE that may be due to weathering processes and modified in estuarine systems (Nesbitt, 1979; Goldstein and Jacobsen, 1988; Ma et al., 2007). La represents an LREE that is immune to change due to modifications in its redox conditions and highly precise and exact INAA values. For these reasons, Sm represents the MREE subgroup. Yb represents the HREE subgroup as it has not only greater accuracy and precision than Lu (according to INAA) but also concentrations between six and eight times higher, thereby enabling more precise results in the application of normalized ratios.

$[\text{La}/\text{Sm}]_{\text{UCC}}$ values, representing the fractionation between LREE and MREE, ranged from 0.71 to 1.39 and averaged 1.00. We found values above 1.00 in 38% of our samples — at stations 17 (1.39), R6 (1.32), 1 (1.22), MC5 (1.15), MC1 (1.10), MC4 (1.09), MC3 (1.07), R1 (1.07), R3 (1.06), 11 (1.04), R2 (1.02), and MC2 (1.00). The sea stations adjacent to the Icapara bar showed values below 1.00 and the sea stations adjacent to the Cananéia bar, values above 1.00, thus evincing different marine influences in the northern and southern regions of the system.

$[\text{La}/\text{Yb}]_{\text{UCC}}$, which represents the fractionation between LREE and HREE, showed values from 0.80 to 1.67. We found HREE enrichment ($[\text{La}/\text{Yb}]_{\text{UCC}} < 1.00$) in stations with high Hf/Al values, indicating the presence of heavy minerals (e.g., MC2, MY2, MY3, 4A) and in those under high hydrodynamic conditions without fine sediments (e.g., 1, 10, 18). According to Jacobsen (1988), the terrestrial input from rivers to oceans is depleted in HREE in relation to LREE; corroborated by the fact that we only obtained $[\text{La}/\text{Yb}]_{\text{UCC}}$ values below 1.00

in some stations in the sea adjacent to northern and southern CIELC and in the internal stations under great influence of its bars.

$[\text{Sm}/\text{Yb}]_{\text{UCC}}$ values, which represent the fractionation between MREE and HREE, ranged from 0.76 to 1.68. The distribution of values resembled those obtained for the $[\text{La}/\text{Yb}]_{\text{UCC}}$ ratio

($r=0.80$; see Table S7 and Figure 7a), in which we found values above 1.00 in 76% of our samples, at stations R1, R2, R3, R6, MY2, MY3, MY4, 2 to 9, 11–18, and MC1. We observed values below 1.00 at stations MC2 (0.99), MC3 (0.98), R4 (0.92), MY1 (0.91), MC4 (0.88), 10 (0.85), MC5 (0.78), and 1 (0.76).

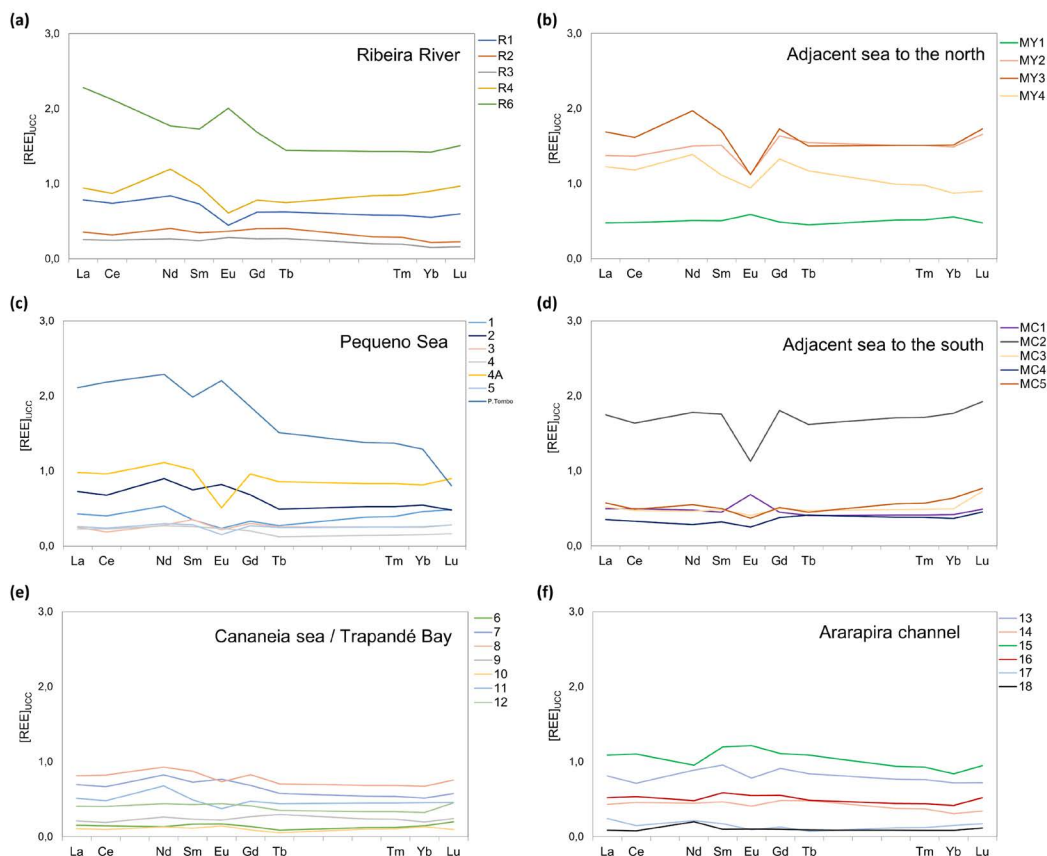


Figure 6. REE* distribution patterns normalized by UCC for surface sediments sampled in several CIELC sectors: Ribeira River (a), adjacent northern sea (b), Pequeno Sea (c), adjacent southern sea (d), Cananeia sea/Trapandé Bay (e), and the Ararapira channel (f).

Ce AND Eu ANOMALIES

Ce anomalies in sediments are usually related to the oxidation of Ce^{+3} to the least soluble Ce^{+4} , resulting in negative anomalies in estuarine and marine waters and positive anomalies in the sediments below them. Sholkovitz (1993) indicated that this phenomenon occurs in two distinct estuarine regions: those with low salinity, in which pH changes are the main factors in the oxidation of Ce^{+3} into the less soluble Ce^{+4} , which promotes a more extensive removal of this element

from the waters than its trivalent neighbors, being adsorbed to fluvial colloids that will undergo estuarine flocculation and coagulation in mixing zones; and in more saline regions (salinity > 20), in which the oxidation of Ce^{+3} into Ce^{+4} can be biologically mediated in more productive sites. We found $[\text{Ce}/\text{Ce}^*]_{\text{UCC}}$ values from 0.63 to 1.06, which were positive at stations 15 (1.06), 16 (1.06), R6 (1.05), 14 (1.04), P. Tombo (1.01), and 6 (1.00). The slightly positive anomalies we observed at the R6 and P. Tombo stations are probably associated

with the oxidation and adsorption processes of Ce^{+4} into fluvial colloids (which occurs along the riverside due to its predominantly alkaline waters), whereas the values we observed at stations 6, 14, 15, and 16 may also be associated with the biologically mediated oxidation of Ce^{+3} into Ce^{+4} . This stems from the higher productivity of these stations, which is associated with high levels of light penetration (low k values) and high values of chlorophyll-*a*. The negative anomalies of Ce in most stations could be associated with two concomitant causes. The first is the removal of Ce by oxidation and its consequent adsorption into the colloids in the water column, followed by its deposition along the Ribeira River. This assumption is supported by the higher value of $[Ce/Ce^*]_{UCC}$ at station R6 than at the P. Tombo one. The second is that the composition of the main rock sources that gave rise to sediments could have negative Ce anomalies, which could result in $[Ce/Ce^*]_{UCC}$ values below 1.00, even in sediments with little or no silt and clay fraction content.

Eu anomalies have higher amplitudes than Ce ones, ranging from 0.56 to 1.56. Positive Eu anomalies may relate to different phenomena. We found strong positive anomalies in sandy samples, i.e., MY1 (1.19), 6 (1.15), 10 (1.42), and MC1 (1.52), which had a degree of selection ranging from moderately selected to well selected and may indicate increased levels of potassic feldspars and plagioclase in these stations. Eu^{+2} is compatible with this mineral during magmatic differentiation, in contrast to trivalent REE (Henderson, 1984). Tessler and Furtado (1983) observed an increase in the concentration of feldspathic grains in the Pleistocene sandy sediments of the Cananéia Formation—i.e., the rupture zone and shallow platform in the studied area—reinforcing this hypothesis. Positive $[Eu/Eu^*]$

UCC also occurs in samples with a higher content of fine sediments, such as in R6 (1.18), 2 (1.18), P. Tombo (1.15), and 15 (1.06). According to Erel and Stolper (1993), slight Eu anomalies in sediments occur as a consequence of the Eu organic-binding constant with oxyhydroxides exceeding those observed for their Sm and Gd neighbors. Benes et al. (2003) associated Eu positive anomalies with the low dissociation rate of Eu -humic compounds in slightly alkaline hydrogen ionic potentials common in estuaries. As the organic matter and iron and manganese oxyhydroxides play an important role in the adsorption of REE and other trace elements to particle surfaces and since Eu has a higher binding affinity to these substrates than other REE—as per Benes et al. (2003)—estuarine sediments with substantial amounts of clays and organic matter availability tend to show positive Eu anomalies. However, note that such northern stations showed more pronounced Eu anomalies than station 15, in southern CIELC.

Stations MC2, MY2, MY3, MY4, 4A, and R1 showed strong negative Eu anomalies (Figure 6). These stations, enriched in REE in relation to UCC , had Hf/Al ratios indicating the presence of heavy minerals. We also observed negative Eu anomalies at R4, MY4, 1, 3, 4A, 5, 8, 9, 11, 13, 14, 17, MC4, MC4, and MC5.

Our Spearman matrix shows the correlation coefficients for these parameters, which we used to evaluate the extent of the linear relationship between ratios and anomalies (Table S8). We used these results several to plot the listed variables as dispersion diagrams and employed the parameters that could modify their values as Hf/Al ratios change to verify individual distribution patterns and relate them to ordinal qualitative variables, such as the degree of sediment selection (Figure 7).

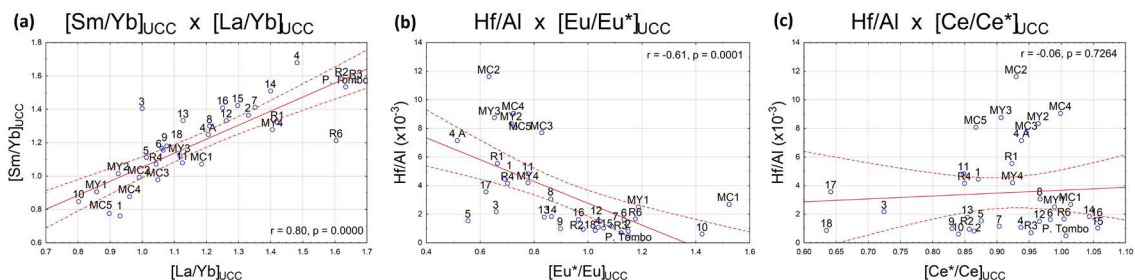


Figure 7. Scatter diagrams showing several REE ratios, namely $[Sm/Yb]_{UCC} \times [La/Yb]_{UCC}$ (a), $Hf/Al \times [Eu/Eu^*]_{UCC}$ (b), and $Hf/Al \times [Ce/Ce^*]_{UCC}$ (c), for CIELC and adjacent sea surface sediments.

The observed non-significant correlation between $[\text{Eu}/\text{Eu}^*]_{\text{UCC}}$ and $[\text{Ce}/\text{Ce}^*]_{\text{UCC}}$ ($r=0.35$, Table S8) indicates that the processes causing such anomalies are unrelated. While $[\text{Eu}/\text{Eu}^*]_{\text{UCC}}$ shows a significantly negative and strong correlation coefficient with the Hf/Al ratio ($r=-0.61$, Table S8 and Figure 7b), $[\text{Ce}/\text{Ce}^*]_{\text{UCC}}$ has no significant correlation with the Hf/Al ratio ($r=0.06$, Table S8 and Figure 7c).

Although we found the highest CIELC ΣREE^* values in stations with a predominantly fine granulometric composition (R6 and P. Tombo), we also observed enrichment in relation to UCC values at stations R1, R4, MY2, MY3, MY4, 4A, and MC2, which showed predominantly sandy sediments and whose Hf/Al ratios indicated heavy mineral enrichment. While R6 and P. Tombo showed LREE enrichment ($[\text{La}/\text{Yb}]_{\text{UCC}}=1.60$ and 1.63, respectively), positive Eu anomalies (1.21

and 1.18, respectively), and Ce positive anomalies (1.05 and 1.01, respectively), stations with heavy mineral enrichment showed values for $[\text{La}/\text{Yb}]_{\text{UCC}}$ from 0.89 (R4) to 1.42 (R1) and strongly negative Eu anomalies from 0.56 (4A) to 0.80 (MY2), and negative Ce anomalies from 0.82 (R4) to 0.97 (MY2).

REE SIGNATURES IN HEAVY MINERALS AT CIELC

Potentially REE-enriched heavy minerals are involved in the observed REE distribution patterns and in the natural processes promoting such patterns, as previously evinced. Tessler (1988) surveyed the presence of heavy minerals throughout CIELC. We compared these data with evinced REE constitution patterns in each possible heavy mineral that could cause such enrichment (Table 1).

Table 1. Summary of the heavy minerals enriched in REE with reported occurrence in sediments by previous authors in the studied area.

Heavy mineral	Average content in the region (%) ^a	ΣREE content ^b	Main elements in the composition ^b	Main REE characteristics ^b
Alanite	-	~18%	Ca, Al, Fe, Si, Hf	LREE enrichment, mainly La and Ce
Apatite	-	1 to 12%	Ca 40%, P 18%	LREE enrichment, negative Eu anomaly, positive Ce anomaly
Augite	< 0.5%	~ 1%	Ca, Mg, Fe, Si, Al	HREE enrichment, positive Eu anomaly
Garnet	~ 3.0%	0.5 to 4%	Mg, Ca, Fe, Al, Cr, Hf	HREE Enrichment, negative Eu anomaly, positive Ce anomaly
Hyperstene	< 2%	~ 2%	Mg 10%, Fe 25%, Si 25%	HREE Enrichment, positive Eu anomaly
Hornblende	~ 15%	-	Si, Al, Ca, Fe, Mg	MREE enrichment followed by LREE enrichment
Ilmenite	~ 1.5%	10 to 200 mg kg ⁻¹	Fe 37%, Ti 32%	Equally enriched in all REE
Monazite	< 0.5 %	~ 56%	Th 5%, P 13%	LREE enrichment (especially La), negative Eu anomaly
Titanite	< 0.5 %	~ 4%	Ti 18%, Ca 19%	LREE enrichment
Zirconite	~ 22%	~ 4%	Th, Zr 43%, Hf 5%, Si 15%	HREE enrichment, negative Eu anomaly

^a relative content of each heavy mineral considering the total assembly of heavy minerals. Values calculated from Tessler (1988); ^b composition in ΣETR and other major elements in the minerals obtained from "Mineralogy Data Base" (www.mindat.org), Yang et al. (2002) for apatite, Jang and Naslund (2003) and Karimpour et al. (2009) for ilmenite, and complemented with observations by Clark (1984).

Among the main minerals that cause REE enrichment in certain sectors of the estuary, we can disregard apatite and alanite because they are depleted in Th. Moreover, REE and Th enrichments are strongly associated (Figure 5i). Moreover, alanite also shows a remarkable enrichment in LREE, mainly in Ce (positive Ce anomalies), which was absent in the studied sediments with high Hf/Al ratios, indicating the presence of heavy minerals.

Hypersthene is a heavy mineral that preferentially incorporates HREE. However, it generally shows a remarkable positive Eu anomaly, making it unlikely that it be an important enricher of REE in CIELC since high Hf/Al stations show strongly negative $[Eu/Eu^*]_{UCC}$. Although present in most samples in Tessler (1988), we considered the verified concentrations as low and this mineral as very rare in the environment according to Gianini's (1987) classification.

Ilmenite had low concentrations in REE (from 10 to 200 mg kg⁻¹) for the values we observed in the sediments enriched in REE and heavy minerals.

Titanite, enriched mainly in Ti, Ca, and REE, has a low abundance throughout the system, with values always below 1% of the total heavy mineral assembly (Tessler, 1988), and a characteristic of enrichment of LREE in relation to HREE (mainly lanthanum), an absent circumstance in samples in which Hf/Al ratios indicated heavy mineral enrichment.

According to Tessler (1988), garnet has an average local abundance of about 3%. Such mineral is strongly enriched in HREE and shows negative Eu and positive Ce anomalies, an absent circumstance in sediments enriched in heavy minerals.

Zirconite, a mineral present in many igneous rocks as the primary product of crystallization, in metamorphic rocks as recrystallized grains, and in sedimentary rocks as detrital grains, is the main candidate for heavy mineral action on the REE anomalies in this study. It has a content enriched in REE, Th, and U, with a strong negative anomaly for Eu and enrichment in HREE with respect to LREE. The significant correlation coefficient, positive and strong between Th and REE (> 0.92 for all REE)—except for Eu ($r=0.88$, Table S5)—supports this assumption. Zirconite also shows elevated $[Lu]_{UCC}$ contents in relation to $[Yb]_{UCC}$, $[Tm]_{UCC}$, and $[Tb]_{UCC}$, which we observed in all samples with high Hf/Al

ratios. Tessler (1988) found zirconite in all samples, including those from the Cananeia Formation, the coastal cords, the intertidal bands, the sandstones (0–10 m deep), and the shallow platform (10–50 m deep) of the studied region, averaging 22% of the total assembly of heavy minerals.

Monazite, which is enriched in REE and Th, may explain the high abundance of REE in the studied area. However, as per Tessler (1988), it shows low concentrations, generally constituting less than 0.5% of the total assembly of heavy minerals. Th enrichment and a slight enrichment of LREE can be expected at stations whose Hf/Al ratios indicate the enrichment of heavy minerals if monazite is an important mineral acting on the enrichment of REE. We found Th enrichment in relation to REE at stations MY2 and MY3 (Figure 5 i) and less negative Eu anomalies than those at station MC2, which may, for example, indicate that such mineral has secondary influence on REE distribution, especially in the sea adjacent to northern CIELC.

As a result, zirconite, containing considerable quantities Zr, Hf, and Th, is the heavy mineral that probably acts more intensely in the distribution of REE concentrations in the sediments of the studied area, which may also receive occasional contributions from monazite due to its high concentration in REE, with Th enrichment relative to the REE when compared to zirconite, leading to a slight difference in the REE×Th diagram (as previously found), and also small quantities of garnet, though insufficient to raise the values of $[Ce/Ce^*]_{UCC}$, which are negative in all samples whose Hf/Al ratio indicates heavy mineral enrichment.

IMPLICATION TO SEDIMENTARY PROVENANCE

We used a diagram with the found values, as proposed by Allègre and Michard (1974). The projection of the values of the La/Yb ratio and values of Σ REE enables us to identify the types of matrix rock of the sediments (Figure 8).

The stations with $[\Sigma REE^*/Al]_{UCC}$ above 2.0 (i.e., R4, MY2, MY3, MY4, and MC2) are in the group that includes sedimentary rocks, granitic rocks, and alkaline basalts, whereas R6 and P. Tombo mostly have granitic sediments. The former sample group showed high Hf/Al ratios and negative Eu anomalies, suggesting detrital content, whereas R6 and P.

Tombo receive important amounts of sediments with chemical properties due to the weathering of the extensive area of granitic rocks in the Ribeira River basin. Station 15, under the influence of both granites and metasedimentary rocks such as

gneisses, phyllites, and mica schists, showed a granite composition influenced by alkaline basalts. For the other samples, dispersion indicates that the matrix rock is predominantly sedimentary with quartz and/or feldspar enrichment, diluting Σ REE.

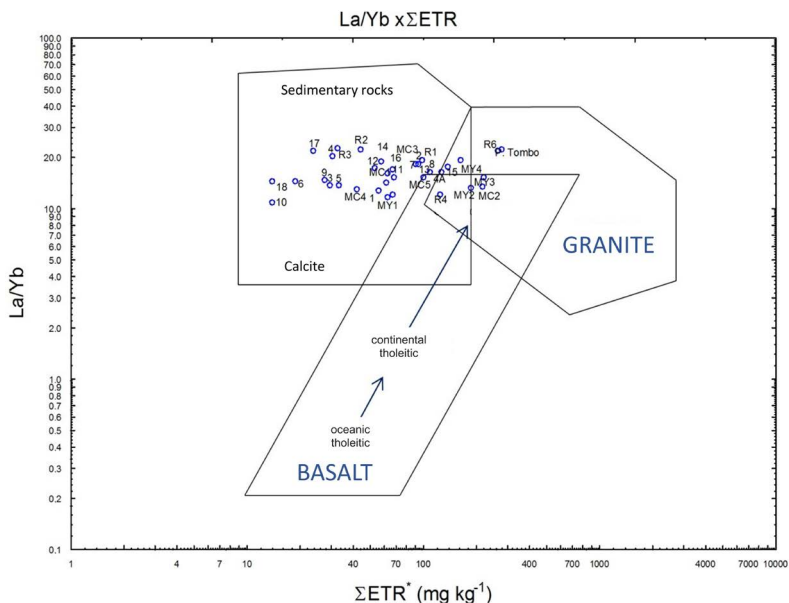


Figure 8. The $\text{La}/\text{Yb} \times \Sigma\text{ETR}^*$ dispersion diagram used to evaluate the type of source rock of the sampled CIELC surface sediments. We shifted box positions according to ΣREE^* percentages, corresponding to 89% of ΣREE (in mg kg^{-1}) according to UCC values.

Feldspars are easily altered minerals whose presence indicates immature sediments with sources close to their current location (Nesbitt and Young, 1982). They also show a high positive Eu anomaly, which we observed at the sandy content stations R3, MY1, and 6 and especially at stations 10 and MC1, as previously reported. Stations R3 and MY1 lied near an outcrop of the crystalline basement (granite-syenitic) at the north of the municipality of Iguape. Such a structure may give rise to the feldspathic material indicated by REE geochemistry. The region of stations 10 and MC1 has a crystalline basement outcrop in eastern Cardoso Island; an area with a mountainous relief composed of granite-syenitic rocks and occupying an area of 86 km^2 with a maximum elevation of 814 m (Weber, 1998). Positive Eu anomalies at stations 10 and MC1 were much higher than those at R3, MY1, which may suggest a closer proximity to the matrix rock. São João hill, spanning about 1.8 km^2 and with a maximum height of 137 m, is

in the urban part of the municipality of Cananéia, whereas Morrete hill, spanning about 0.4 km^2 and with a maximum height of 47 m, is in the Ilha Comprida neighborhood (Spinelli and Gomes, 2008). Despite their small size, these hills could potentially supply feldspar material for the region as it is completely flat. Such outcrops are actually the body of a single interconnected rock under the Cananéia sea (Suguio et al., 1987). However, stations 8 and 9, which are closer to this rock, have no positive Eu anomalies, which may suggest that such an alkaline intrusion has little ability to supply feldspars to the adjacent submerged region.

Granites from the crystalline basement, which also appear near the bridge across the Aroeira River crossing the Cubatão channel, may be related to the positive Eu anomalies in sandy sediments, indicating the presence of feldspars in the station 6 region.

The R6 station lied in the deepest part of the shallow area that predominantly concentrates the

fine sediments of the Ribeira River, whereas the sediments at the P. Tombo station consist of fine sediments from the Ribeira River and chemical sediments from the interaction of fluvial and marine waters. Eu positive anomalies in these stations may be associated with the formation of Eu-organic complexes and positive Ce anomalies are probably associated with their oxidation into Ce⁺⁴, which is less soluble as a function of the elevation of pH values, as previously reported.

To complement the evaluation of REE levels, fractionation, and anomalies in this study, we compared our data to those reported for other coastal systems in Brazil and around the world. We chose studies that determined REE in total sediment and showed raw elemental analysis results for this comparison as they would enable us to calculate the fractionation and anomalies of REE in the same manner as in this study. Table 2 shows Σ REE concentration intervals and $[La/Yb]_{UCC}$, $[Ce/Ce^*]_{UCC}$, and $[Eu/Eu^*]_{UCC}$ ratios. We normalized the data in these related studies using the values of the UCC for comparison whenever necessary.

Regarding Σ REE, CIELC showed the highest value range of all evaluated environments. Our

average Σ REE* value resembled that in Marmolejo-Rodrigues et al. (2007) for the Marabasco River and its estuarine system. However, the great variability indicates a more heterogeneous composition for the CIELC sediments. All authors in Table 2 reported that REE content was strongly and positively correlated with that of silt and clay in sediments. Among the cited studies, only Oliveira et al. (2007) showed solely positive $[Ce/Ce^*]_{UCC}$, which the authors attributed to the oxidation of Ce⁺³ into Ce⁺⁴ at the interface of the river with the estuary. Marmolejo-Rodrigues et al. (2007) showed the highest $[Eu/Eu^*]_{UCC}$ values, which they found at stations near tectonic and volcanic regions. However, the authors observed slightly negative Eu anomalies in most sediment samples and indicated that these could stem from the weathering of intrusive rocks containing iron ore. The greatest enrichment of LREE in relation to HREE occurred in sediments from the Huelva ria (Borrego et al., 2004) and the Santos-S. Vicente estuarine systems (Oliveira et al., 2007). Prajith et al. (2015) found positive Eu anomalies in all Mandovi estuary sediments, strongly positive Fe-Mn ore anomaly, and feldspathic enrichment in sandy sediments in the outermost sections of that estuary.

Table 2. Intervals (maximum and minimum) of Σ REE values, in mg Kg⁻¹, and normalized ratios $[La/Yb]_{UCC}$, $[Ce/Ce^*]_{UCC}$, and $[Eu/Eu^*]_{UCC}$ in several studies and regions of the Brazil and the world. Normalization with raw data and values for the Upper Continental Crust.

Studied region	Σ REE		$[La/Yb]_{UCC}$		$[Ce/Ce^*]_{UCC}$		$[Eu/Eu^*]_{UCC}$		Quantification method	References
	Min	Max	Min	Max	Min	Max	Min	Max		
CIELC, Brazil	14.3	285.0	0.80	1.67	0.63	1.06	0.56	1.56	INAA	This study*
Santos-S. Vicente (Brazil)	194	254	1.43	2.47	1.09	1.21	0.54	0.82	INAA	Oliveira et al., 2007** (no phosphogypsum contamination)
Marabasco estuary, Mexico	27.5	157.0	0.49	1.64	0.88	0.94	0.81	2.22	INAA	Marmolejo-Rodriguez et al., 2007
Vigo ria – Pontevedra, Spain	2.0	220.0	0.65	2.29	0.71	1.00	0.79	1.41	ICP-MS	Prego et al., 2009
Mandovi estuary, western India	37.1	160.4	0.49	0.91	0.77	1.77	1.27	1.76	ICP-MS	Prajith et al., 2015
Bohai Bay, China	97.6	202.0	0.86	1.00	0.89	1.03	1.14	1.51	ICP-MS	Zhang et al., 2014
Huelva Ria, Spain	36.0	197.7	0.80	3.26	0.80	1.43	0.93	1.18	ICP-MS	Borrego et al., 2004 (no phosphogypsum contamination)
Johore straight, Malaysia	36.0	162.0	0.99	1.75	0.44	2.04	-	-	INAA	Yusof et al., 2001***

* in this study, Σ REE = Σ REE*;

** in Oliveira et al. (2007), Σ REE = (La+Ce+Nd+Sm+Eu+Tb+Yb+Lu);

*** in Yusof et al. (2001), Σ REE = (La+Ce+Sm+Eu+Tb+Dy+Y).

PHOSPHOGYPSUM: A RISK FOR CIELC?

Phosphogypsum is an acid by-product of industries that produce phosphate fertilizers and it is extracted during the production of phosphoric acid from phosphate rocks. It mainly consists of calcium sulfate (gypsum) and impurities, whose composition is greatly influenced by the used phosphate rock matrix (Rutherford et al., 1995; Hull and Burnett, 1996; Al-Masri et al., 2004). It shows high levels of fluoride, certain naturally occurring radionuclides, and trace elements (including Ag, Ba, Cd, and REE). Hence the concern that such materials may negatively impact the environment (Rutherford et al., 1994; Saueia et al., 2012). REE have been widely used to examine environmental contamination due to phosphogypsum (e.g. Borrego et al., 2004; Silva et al., 2005; Oliveira et al., 2007) and acid mine drainage (Elbaz-Poulichet and Dupuy, 1999; Johannesson and Zhou, 1999).

Several companies in the Ribeira Valley have explored phosphate rocks since 1938, especially in the municipality of Cajati. Phosphate rocks are extracted from igneous carbonatites. The main company (Vale) is located on the banks of the Jacupiranguinha River on the lower course of the Ribeira River.

To verify the possible arrival of material from fertilizer production to CIELC, we conducted an elemental measurement of two samples of by-products of fertilizer production at Vale. We obtained Cajati phosphogypsum (CP) from one of the open-air phosphogypsum piles belonging to the company on March 10, 2014. We also obtained a sample from a settling tank (ST) in May 2015 by placing a Van Veen-type catcher directly into the stream that transports waste from phosphoric acid production process to decantation tanks. We analyzed these samples following the same criteria we adopted for other sediment samples in this study.

CP showed high levels of carbonate (35.3%). Ca^{+2} and SO_4^{-2} are the main components of phosphogypsum, accounting for up to 90% of this by-product (Rutherford et al., 1994). The enrichment of REE with respect to UCC values was La (8.6), Ce (9.2), Nd (12.0), Sm (11.3), Eu (15.5), Gd (10.9), Tb (6.4), and Lu (1.6). Yb showed values close to those for UCC. We found great fractionation and enrichment of LREE ($[\text{La}/\text{Yb}]_{\text{UCC}}=7.15$), especially

of MREE ($[\text{Sm}/\text{Yb}]_{\text{UCC}}=9.40$) in relation to HREE, and an important positive $[\text{Eu}/\text{Eu}^*]_{\text{UCC}}$ (1.56). We observed a slightly negative $[\text{Ce}/\text{Ce}^*]_{\text{UCC}}$ (0.95) and $[\text{Sm}/\text{Nd}]_{\text{UCC}}$ (0.94) (Figure 9) and the depletion of Al (0.5) and Th (0.4).

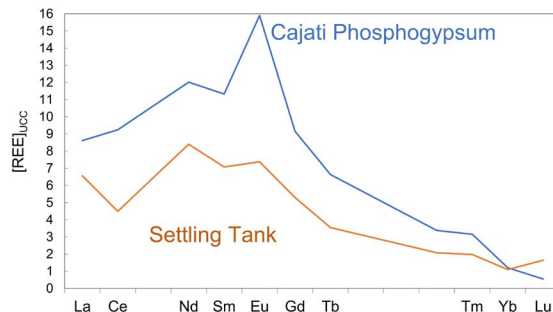


Figure 9. REE distribution patterns normalized by continental crust values (UCC) for the Cajati phosphogypsum (CP) and settling tank (ST).

ST had 45.1% of carbonates, with enrichment of the REE* La (6.6), Ce (4.5), Nd (8.4), Sm (7.1), Eu (7.2), Gd (5.1), Tb (3.4), and Lu (1.6). As with the CP sample, ST also showed Al (0.7) and Th (0.4) depletion. We observed a 5.97 and 9.40 $[\text{La}/\text{Yb}]_{\text{UCC}}$ and $[\text{Sm}/\text{Yb}]_{\text{UCC}}$ ratios, respectively, a positive Eu anomaly (1.21), and a negative $[\text{Ce}/\text{Ce}^*]_{\text{UCC}}$ (0.63), agreeing with our CP findings.

Station R6, whose silt and clay content indicates depositional conditions favorable to the accumulation of chemical sediments, resembled the CP sample the most, i.e., (i) the highest carbonate content of all sampled sediments (except for those near *sambaquis*); (ii) the enrichment of LREE and MREE over HREE; (iii) positive Eu anomalies (the highest among the samples with relevant fine fractions); (iv) Al values below those predicted by the linear regression regarding silt and clay content (Figure 5a); (v) Th values below those predicted by the regression with REE (Figure 5i); and (vi) higher Al-normalized $[\text{REE}/\text{Al}]_{\text{UCC}}$ among samples that outside the influence of detrital heavy minerals (2.41). The P. Tombo station also has most of the characteristics of the R6 station but its $[\text{REE}/\text{Al}]_{\text{UCC}}$ totals 1.58, placing it below the value at which we could consider it moderately contaminated. Note that this station is in an environmentally sensitive part of CIELC.

Other authors have also found Zn and Pb enrichment (e.g., Tramonte et al., 2016) near station

R6. This probably relates to mineral exploration, increasing the likelihood of it receiving sediments from anthropogenic activities (including the exploration of phosphogypsum in Cajati) in the drainage of the Ribeira River basin or undergoing their influence.

The current context of global land use changes, increasing demand for fertilizers, and the use of REE in various technological products has altered how humanity concentrates and eliminates these elements in its daily life. Studies must be carried out in regions near industrial units (especially in the Jacupiranguinha and Jacupiranga River sediments) as they have lacked the adequate attention on the potential impacts of such activities.

CONCLUSION

This study showed the sedimentary distribution of REE in CIELC and two contiguous domains to better evaluate the natural processes and anthropogenic signals that can endanger the quality of this system. Surface sediments showed characteristics strongly related to multiples active processes, with a marked influence of depositional conditions and an important contribution of the local lithology on sediment geochemistry. Sedimentary textural characteristics, depositional conditions, the ratios of certain elements, REE abundances, enrichments, normalized values, fractionations, anomalies, complementary environmental information, water properties and hydrodynamics, and historic and recent human regional activities enable the determination of natural enrichments of REE in relation to UCC values due to the presence of heavy minerals (mainly zirconite, followed by monazite), which are distributed as a function of hydrodynamic selection in CIELC (especially in its external contiguous domains). We also found that other minerals act in REE distribution in the system, such as feldspar and its presence in specific regions close to its source. Only one sample in the northern part of the estuary (R6) showed REE enrichment unrelated to the distribution of heavy minerals and several convergent characteristics with the analyzed phosphogypsum samples, suggesting environmental contamination. Other authors have also indicated that the area was contaminated with Zn and Pb from mining processes along the Ribeira

River basin. This region, in which some of the fine sediments stemming from continental processes are deposited, deserves special attention from environmental authorities.

ACKNOWLEDGMENTS

This study integrated projects FEBIOGEOQUIM (CNPq 478-890/2011-7) and INCT-TMCOcean (CNPq 573-601/2008-9). The authors would like to thank Dr. Cassiana Seimi Nomura, Dr. Pedro Vitoriano, and Dr. Flávio Leme from the Chemistry Institute of University of São Paulo for making it possible to analyze metals using LIBS and Dr. Michel Michaelovitch de Mahiques for allowing the use of the Malvern Mastersizer 2000. We also thank Dr. Bárbara Paci Mazzilli, from the National Council of Nuclear Energy – Nuclear and Energy Research Institute, for donating the sample of Cajati Phosphogypsum used in this study. The authors thank the anonymous reviewers and the editor for their valuable comments and suggestions to improve the quality of this manuscript.

AUTHOR CONTRIBUTIONS

V.G.C.: Investigation, Methodology, Formal Analysis, Data Curation, Writing - Original Draft, Writing – Review and Editing, Conceptualization.

D.I.T.F.: Methodology; Data Curation, Supervision.

E.S.B.: Supervision; Resources; Project Administration; Writing – Review and Editing.

REFERENCES

- Allègre, C. & Michard, G. 1974. *Introduction to Geochemistry. Geophysics and astrophysics monographs* (Vol. 10). Boston: Reidel Publishing Company.
- Al-Masri, M. S., Amin, Y., Ibrahim, S. & Al-Bich, F. 2004. Distribution of some trace metals in Syrian phosphogypsum. *Applied Geochemistry*, 19(5), 747–753. DOI: <https://doi.org/10.1016/j.apgeochem.2003.09.014>
- Almeida, F. F. M. 1976. The system of continental rifts bordering the Santos Basin. *Brazilian Academy of Sciences*, 48, 15–26.
- Armstrong-Altrin, J., Lee, Y., Kasper-Zubillaga, J., Carranza-Edwards, A., Garcia, D., Eby, G., Balaran, V. & Cruz-Ortiz, N. 2012. Geochemistry of beach sands along the western Gulf of Mexico, Mexico: Implication for provenance. *Geochemistry*, 72(4), 345–362. DOI: <https://doi.org/10.1016/j.chemer.2012.07.003>
- Balashov, Y. A., Ronov, A. B., Migdisov, A. A. & Turanskaya, N. V. 1964. The effect of climate and facies environment in the fractionation of the rare earths during sedimentation. *Geochemistry International*, 10, 951–969.

- Barcellos, R. L., Berbel, G. B. B., Braga, E. S. & Furtado, V. V. 2005. Distribuição e características do fósforo sedimentar do Sistema Estuarino Lagunar Cananéia-Iguape, Estado de São Paulo, Brasil. *Geochimica Brasiliensis*, 19(1), 22–36.
- Barcellos, R. L., Camargo, P. B., Galvão, A. & Weber, R. R. 2009. Sedimentary organic matter in cores of the Cananéia-Iguape lagoonal-estuarine system, São Paulo estate, Brazil. *Journal of Coastal Research*, (56), 1335–1339.
- Bau, M. 1999. Scavenging of dissolved yttrium and rare earths by precipitating iron oxyhydroxide: experimental evidence for Ce oxidation, Y-Ho fractionation, and lanthanide tetrad effect. *Geochimica et Cosmochimica Acta*, 63(1), 67–77. DOI: [https://doi.org/10.1016/s0016-7037\(99\)00014-9](https://doi.org/10.1016/s0016-7037(99)00014-9)
- Bau, M. & Koschinsky, A. 2009. Oxidative scavenging of cerium on hydrous Fe oxide: Evidence from the distribution of rare earth elements and yttrium between Fe oxides and Mn oxides in hydrogenetic ferromanganese crusts. *Geochemical Journal*, 43(1), 37–47. DOI: <https://doi.org/10.2343/geochemj.1.0005>
- Benes, P., Stamberg, K., Vopalka, D., Siroky, L. & Prochazkova, S. 2003. Kinetics of radioeuropium sorption on Goresben sand from aqueous solutions and groundwater. *Journal of Radioanalytical and Nuclear Chemistry*, 256, 465–472. DOI: <https://doi.org/10.1023/A:1024595515126>
- Bérgamo, A. L. 2000. *Características da hidrografia, circulação e transporte de sal: Barra de Cananéia, Sul do Mar de Cananéia e Baía do Trapandé* (MSc Thesis). Universidade de São Paulo, Agência USP de Gestão da Informação Acadêmica (AGUIA), São Paulo. <https://doi.org/10.11606/d.21.2000.tde-27052004-190010>
- Borrego, J., López-González, N., Carro, B., Grande, J. A., De la Torre, M. L. & Valente, T. M. F. 2012. Rare-earth element fractionation patterns in estuarine sediments as a consequence of acid mine drainage: a case study in SW Spain. *Boletín Geológico y Minero*, 123(1), 55–64.
- Borrego, J., López-González, N., Carro, B. & Lozano-Soria, O. 2004. Origin of the anomalies in light and middle REE in sediments of an estuary affected by phosphogypsum wastes (south-western Spain). *Marine Pollution Bulletin*, 49(11–12), 1045–1053. DOI: <https://doi.org/10.1016/j.marpolbul.2004.07.009>
- Braga, E. S. & Chiozzini, V. G. 2012. Alteration on the nitrogen balance on the Cananéia-Iguape estuarine-lagoon complex (Brazil) in function of the anthropogenic influence. In: *Anais do II Workshop Antropicosta Iberoamerica*. Montevideo.
- Burkov, V. V. & Podporina, E. K. 1967. Rare Earths in the weathering crusts of granitoids: *Doklady Akademii Nauk*, 177, 691–694. DOI: <https://doi.org/10.1007/s12583-014-0449-z>
- Buynevich, I., Fitzgerald, D. & Van Heteren, S. 2004. Sedimentary records of intense storms in Holocene barrier sequences, Maine, USA. *Marine Geology*, 210(1–4), 135–148. DOI: <https://doi.org/10.1016/j.margeo.2004.05.007>
- Byrne, R. & Kim, K.-H. 1990. Rare earth element scavenging in seawater. *Geochimica et Cosmochimica Acta*, 54(10), 2645–2656. DOI: [https://doi.org/10.1016/0016-7037\(90\)90002-3](https://doi.org/10.1016/0016-7037(90)90002-3)
- Calvert, S. & Pedersen, T. F. 2007. Elemental proxies for paleoclimatic and palaeoceanographic variability in marine sediments: interpretation and application. *Developments in Marine Geology*, 1, 567–644. DOI: [https://doi.org/10.1016/S1572-5480\(07\)01019-6](https://doi.org/10.1016/S1572-5480(07)01019-6)
- Chaillou, G., Anschutz, P., Lavaux, G. & Blanc, G. 2006. Rare earth elements in the modern sediments of the Bay of Biscay (France). *Marine Chemistry*, 100(1–2), 39–52. DOI: <https://doi.org/10.1016/j.marchem.2005.09.007>
- CETESB (COMPANHIA DE TECNOLOGIA DE SANEAMENTO AMBIENTAL DE SÃO PAULO). 2013. *Relatório de Qualidade das Águas Interiores do Estado de São Paulo, 2012* (resreport). São Paulo: Secretaria do Meio Ambiente.
- Cunha-Lignon, M. 2001. *Dinâmica do Manguezal no Sistema Cananéia-Iguape, Estado de São Paulo – Brasil*. (mathesis). Instituto Oceanográfico, Universidade de São Paulo, São Paulo.
- Dellwig, O., Hinrichs, J., Hild, A. & Brumsack, H.-J. 2000. Changing sedimentation in tidal flat sediments of the southern North Sea from the Holocene to the present: a geochemical approach. *Journal of Sea Research*, 44(3–4), 195–208. DOI: [https://doi.org/10.1016/s1385-1101\(00\)00051-4](https://doi.org/10.1016/s1385-1101(00)00051-4)
- Elbaz-Poulichet, F. & Dupuy, C. 1999. Behaviour of rare earth elements at the freshwater–seawater interface of two acid mine rivers: the Tinto and Odiel (Andalucia, Spain). *Applied Geochemistry*, 14(8), 1063–1072. DOI: [https://doi.org/10.1016/s0883-2927\(99\)00007-4](https://doi.org/10.1016/s0883-2927(99)00007-4)
- Elderfield, H., Upstill-Goddard, R. & Sholkovitz, E. 1990. The rare earth elements in rivers, estuaries, and coastal seas and their significance to the composition of ocean waters. *Geochimica et Cosmochimica Acta*, 54(4), 971–991. DOI: [https://doi.org/10.1016/0016-7037\(90\)90432-k](https://doi.org/10.1016/0016-7037(90)90432-k)
- Elias, Md. S., Ibrahim, S., Samuding, K., Kantasamy, N., Rahman, S. & Hashim, A. 2019. Rare earth elements (REEs) as pollution indicator in sediment of Linggi River, Malaysia. *Applied Radiation and Isotopes*, 151, 116–123. DOI: <https://doi.org/10.1016/j.apradiso.2019.05.038>
- Erel, Y. & Stolper, E. 1993. Modeling of rare-earth element partitioning between particles and solution in aquatic environments. *Geochimica et Cosmochimica Acta*, 57(3), 513–518. DOI: [https://doi.org/10.1016/0016-7037\(93\)90363-2](https://doi.org/10.1016/0016-7037(93)90363-2)
- Fiket, Ž., Mikac, N. & Kniewald, G. 2017. Influence of the geological setting on the REE geochemistry of estuarine sediments: A case study of the Zrmanja River estuary (eastern Adriatic coast). *Journal of Geochemical Exploration*, 182, 70–79. DOI: <https://doi.org/10.1016/j.gexplo.2017.09.001>
- Folk, R.L. & Ward, W.C. 1957. A Study in the Significance of Grain-Size Parameters. *Journal of Sedimentary Petrology*, 27, 3–26.
- Gianini, P. C. F. 1987. *Sedimentação quaternária na planície costeira de Peruibe-Itanhaém (SP)* (mathesis). Instituto de Geociências, Universidade de São Paulo, São Paulo.
- Godwyn-Paulson, P., Jonathan, M., Rodríguez-Espinosa, P. & Rodríguez-Figueroa, G. 2022. Rare earth element enrichments in beach sediments from Santa Rosalia

- mining region, Mexico: An index-based environmental approach. *Marine Pollution Bulletin*, 174, 113271. DOI: <https://doi.org/10.1016/j.marpolbul.2021.113271>
- Goldstein, S. & Jacobsen, S. 1988. REE in the Great Whale River estuary, northwest Quebec. *Earth and Planetary Science Letters*, 88(3–4), 241–252. DOI: [https://doi.org/10.1016/0012-821x\(88\)90081-7](https://doi.org/10.1016/0012-821x(88)90081-7)
- Guimarães, V. & Sígolo, J. B. 2008. Associação de resíduos da metalurgia com sedimentos em suspensão - Rio Ribeira de Iguape. *Geologia USP. Série Científica*, 8(2), 1–10. DOI: <https://doi.org/10.5327/z1519-874x2008000200001>
- Haley, B., Klinkhammer, G. & Mcmanus, J. 2004. Rare earth elements in pore waters of marine sediments. *Geochimica et Cosmochimica Acta*, 68(6), 1265–1279. DOI: <https://doi.org/10.1016/j.gca.2003.09.012>
- Hannigan, R., Dorval, E. & Jones, C. 2010. The rare earth element chemistry of estuarine surface sediments in the Chesapeake Bay. *Chemical Geology*, 272(1–4), 20–30. DOI: <https://doi.org/10.1016/j.chemgeo.2010.01.009>
- Henderson, P. 1984. General Geochemical Properties and Abundances of the Rare Earth Elements. In: Henderson, P. (ed.), *Rare Earth Element Geochemistry* (pp. 1–32). Amsterdam, Netherlands: Elsevier. DOI: <https://doi.org/10.1016/b978-0-444-42148-7.50006-x>
- Hinrichs, J., Dellwig, O. & Brumsack, H. 2002. Lead in sediments and suspended particulate matter of the German Bight: natural versus anthropogenic origin. *Applied Geochemistry*, 17(5), 621–632.
- Hull, C. & Burnett, W. 1996. Radiochemistry of Florida phosphogypsum. *Journal of Environmental Radioactivity*, 32(3), 213–238. DOI: [https://doi.org/10.1016/0265-931x\(95\)00061-e](https://doi.org/10.1016/0265-931x(95)00061-e)
- Humphris, S. 1984. The Mobility of the Rare Earth Elements in the Crust. In: Henderson, P. (ed.), *Rare Earth Element Geochemistry* (pp. 317–342). Amsterdam, Netherlands: Elsevier. DOI: <https://doi.org/10.1016/b978-0-444-42148-7.50014-9>
- Johannesson, K. & Zhou, X. 1999. Origin of middle rare earth element enrichments in acid waters of a Canadian High Arctic lake. *Geochimica et Cosmochimica Acta*, 63(1), 153–165. DOI: [https://doi.org/10.1016/s0016-7037\(98\)00291-9](https://doi.org/10.1016/s0016-7037(98)00291-9)
- Kalis, A., Merkt, J. & Wunderlich, J. 2003. Environmental changes during the Holocene climatic optimum in central Europe - human impact and natural causes. *Quaternary Science Reviews*, 22(1), 33–79. DOI: [https://doi.org/10.1016/s0277-3791\(02\)00181-6](https://doi.org/10.1016/s0277-3791(02)00181-6)
- Kechiched, R., Laouar, R., Bruguier, O., Kocsis, L., Salmi-Laouar, S., Bosch, D., Ameer-Zaimeche, O., Foufou, A. & Larit, H. 2020. Comprehensive REE + Y and sensitive redox trace elements of Algerian phosphorites (Tébessa, eastern Algeria): A geochemical study and depositional environments tracking. *Journal of Geochemical Exploration*, 208, 106396. DOI: <https://doi.org/10.1016/j.gexplo.2019.106396>
- Kolditz, K., Dellwig, O., Barkowski, J., Bahlo, R., Leipe, T., Freund, H. & Brumsack, H.-J. 2012. Geochemistry of Holocene salt marsh and tidal flat sediments on a barrier island in the southern North Sea (Langeoog, North-west Germany). *Sedimentology*, 59(2), 337–355. DOI: <https://doi.org/10.1111/j.1365-3091.2011.01252.x>
- Larsonneur, C., Bouysse, P. & Auffret, J.-P. 1982. The superficial sediments of the English Channel and its Western Approaches. *Sedimentology*, 29(6), 851–864. DOI: <https://doi.org/10.1111/j.1365-3091.1982.tb00088.x>
- Lawrence, M. & Kamber, B. 2006. The behaviour of the rare earth elements during estuarine mixing—revisited. *Marine Chemistry*, 100(1–2), 147–161. DOI: <https://doi.org/10.1016/j.marchem.2005.11.007>
- Leroy, J. & Turpin, L. 1988. REE, Th and U behaviour during hydrothermal and supergene processes in a granitic environment. *Chemical Geology*, 68(3–4), 239–251. DOI: [https://doi.org/10.1016/0009-2541\(88\)90024-1](https://doi.org/10.1016/0009-2541(88)90024-1)
- Liu, J., Xiang, R., Chen, Z., Chen, M., Yan, W., Zhang, L. & Chen, H. 2013. Sources, transport and deposition of surface sediments from the South China Sea. *Deep Sea Research Part I: Oceanographic Research Papers*, 71, 92–102. DOI: <https://doi.org/10.1016/j.dsr.2012.09.006>
- Ma, J.-L., Wei, G.-J., Xu, Y.-G., Long, W.-G. & Sun, W.-D. 2007. Mobilization and re-distribution of major and trace elements during extreme weathering of basalt in Hainan Island, South China. *Geochimica et Cosmochimica Acta*, 71(13), 3223–3237. DOI: <https://doi.org/10.1016/j.gca.2007.03.035>
- Mahiques, M. de, Figueira, R., Salaroli, A., Alves, D. & Gonçalves, C. 2013. 150 years of anthropogenic metal input in a Biosphere Reserve: the case study of the Cananéia-Iguape coastal system, Southeastern Brazil. *Environmental Earth Sciences*, 68(4), 1073–1087. DOI: <https://doi.org/10.1007/s12665-012-1809-6>
- Marmolejo-Rodríguez, A., Prego, R., MEYER-WILLERER, A., SHUMILIN, E. & SAPOZHNIKOV, D. 2007. Rare earth elements in iron oxy-hydroxide rich sediments from the Marabasco River-Estuary System (pacific coast of Mexico). REE affinity with iron and aluminium. *Journal of Geochemical Exploration*, 94(1–3), 43–51. DOI: <https://doi.org/10.1016/j.gexplo.2007.05.003>
- Maulana, A., Yonezu, K. & Watanabe, K. 2014. Geochemistry of rare earth elements (REE) in the weathered crusts from the granitic rocks in Sulawesi Island, Indonesia. *Journal of Earth Science*, 25(3), 460–472. DOI: <https://doi.org/10.1007/s12583-014-0449-z>
- McLennan, S. 1989. Rare earth elements in sedimentary rocks: influence of provenance and sedimentary processes. In: Lipin, D. R. & McKay, G. A. (eds.), *Geochemistry and Mineralogy of Rare Earth Elements* (Vol. 21, pp. 169–200). Berlin: De Gruyter. DOI: <https://doi.org/10.1515/9781501509032-010>
- Miyao, S. Y., Nishihara, L. & Sarti, C. C. 1986. Características físicas e químicas do sistema estuarino-lagunar de Cananéia-Iguape. *Boletim Do Instituto Oceanográfico*, 34, 23–26. DOI: <https://doi.org/10.1590/s0373-55241986000100003>
- Moeller, T. 1985. *The chemistry of the lanthanides*. New York: Pergamon.
- Nesbitt, H. W. 1979. Mobility and fractionation of rare earth elements during weathering of a granodiorite. *Nature*, 279(5710), 206–210. DOI: <https://doi.org/10.1038/279206a0>
- Oliveira, S., Silva, P., Mazzilli, B., Favaro, D. & Saueia, C. 2007. Rare earth elements as tracers of sediment contamination by phosphogypsum in the Santos estuary,

- southern Brazil. *Applied Geochemistry*, 22(4), 837–850. DOI: <https://doi.org/10.1016/j.apgeochem.2006.12.017>
- Pérez-López, R., Macías, F., Cánovas, C., Sarmiento, A. & Pérez-Moreno, S. 2016. Pollutant flows from a phosphogypsum disposal area to an estuarine environment: An insight from geochemical signatures. *Science of The Total Environment*, 553, 42–51. DOI: <https://doi.org/10.1016/j.scitotenv.2016.02.070>
- Prajith, A., Rao, V. & Kessarkar, P. 2015. Controls on the distribution and fractionation of yttrium and rare earth elements in core sediments from the Mandovi estuary, western India. *Continental Shelf Research*, 92, 59–71. DOI: <https://doi.org/10.1016/j.csr.2014.11.003>
- Prego, R., Caetano, M., Vale, C. & Marmolejo-Rodríguez, J. 2009. Rare earth elements in sediments of the Vigo Ria, NW Iberian Peninsula. *Continental Shelf Research*, 29(7), 896–902. DOI: <https://doi.org/10.1016/j.csr.2009.01.009>
- Rao, W., Mao, C., Wang, Y., Huang, H. & Ji, J. 2017. Using Nd-Sr isotopes and rare earth elements to study sediment provenance of the modern radial sand ridges in the southwestern Yellow Sea. *Applied Geochemistry*, 81, 23–35. DOI: <https://doi.org/10.1016/j.apgeochem.2017.03.011>
- Rasmussen, B., Buick, R. & Taylor, W. 1998. Removal of oceanic REE by authigenic precipitation of phosphatic minerals. *Earth and Planetary Science Letters*, 164(1–2), 135–149. DOI: [https://doi.org/10.1016/s0012-821x\(98\)00199-x](https://doi.org/10.1016/s0012-821x(98)00199-x)
- Ribeira de Iguape and South Coast Hydrographic Basin Committee, 2008. Relatório de Situação dos Recursos Hídricos da Unidade de Gerenciamento n. 11: Bacia Hidrográfica do Ribeira de Iguape e Litoral Sul. São Paulo – SP.
- Rolland, Y., Cox, S., Boullier, A.-M., Pennacchioni, G. & Mancktelow, N. 2003. Rare earth and trace element mobility in mid-crustal shear zones: insights from the Mont Blanc Massif (Western Alps). *Earth and Planetary Science Letters*, 214(1–2), 203–219. DOI: [https://doi.org/10.1016/s0012-821x\(03\)00372-8](https://doi.org/10.1016/s0012-821x(03)00372-8)
- Ross, J. L. S. 2002. A morfogênese da Bacia do Ribeira de Iguape e os sistemas ambientais. *GEOUSP – Espaço e Tempo*, 12.
- Rutherford, P., Dudas, M. & Arocena, J. 1995. Radioactivity and Elemental Composition of Phosphogypsum Produced From Three Phosphate Rock Sources. *Waste Management & Research: The Journal for a Sustainable Circular Economy*, 13(5), 407–423. DOI: <https://doi.org/10.1177/0734242x9501300502>
- Rutherford, P., Dudas, M. & Samek, R. 1994. Environmental impacts of phosphogypsum. *Science of The Total Environment*, 149(1–2), 1–38. DOI: [https://doi.org/10.1016/0048-9697\(94\)90002-7](https://doi.org/10.1016/0048-9697(94)90002-7)
- Saueia, C. H. R., Bourlegat, F. M. L., Mazzilli, B. P. & Fávoro, D. I. T. 2012. Availability of metals and radionuclides present in phosphogypsum and phosphate fertilizers used in Brazil. *Journal of Radioanalytical and Nuclear Chemistry*, 297(2), 189–195. DOI: <https://doi.org/10.1007/s10967-012-2361-2>
- Schäfer, J., Coynel, A., Turner, A. & Koch, B. 2016. The 13th International Estuarine Biogeochemistry Symposium: 'Estuaries and bays under anthropogenic pressure: past-present-future'. *Marine Chemistry*, 185, 1–2. DOI: <https://doi.org/10.1016/j.marchem.2016.05.012>
- Schropp, S. J. & Windom, H. L. (eds.). 1988. *Guide to the Interpretation of Metal Concentrations in Estuarine Sediments*. Florida: Florida Department of Environmental Protection.
- Sholkovitz, E. 1993. The geochemistry of rare earth elements in the Amazon River estuary. *Geochimica et Cosmochimica Acta*, 57(10), 2181–2190. DOI: [https://doi.org/10.1016/0016-7037\(93\)90559-f](https://doi.org/10.1016/0016-7037(93)90559-f)
- Shynu, R., Rao, V., Kessarkar, P. & Rao, T. 2011. Rare earth elements in suspended and bottom sediments of the Mandovi estuary, central west coast of India: Influence of mining. *Estuarine, Coastal and Shelf Science*, 94(4), 355–368. DOI: <https://doi.org/10.1016/j.ecss.2011.07.013>
- Silva, P., Mazzilli, B. & Fávoro, D. 2005. Distribution of U and Th decay series and rare earth elements in sediments of Santos Basin: correlation with industrial activities. *Journal of Radioanalytical and Nuclear Chemistry*, 264, 449–455. DOI: <https://doi.org/10.1007/s10967-005-0736-3>
- Slukovskii, Z., Guzeva, A. & Dauvalter, V. 2022. Rare earth elements in surface lake sediments of Russian arctic: Natural and potential anthropogenic impact to their accumulation. *Applied Geochemistry*, 142, 105325. DOI: <https://doi.org/10.1016/j.apgeochem.2022.105325>
- Souza, L. A. P., Tessler, M. G. & Galli, V. L. 1996. O gráben de Cananéia. *Revista Brasileira de Geociências*, 26(3), 139–150. DOI: <https://doi.org/10.25249/0375-7536.1996139150>
- Su, N., Yang, S., Guo, Y., Yue, W., Wang, X., Yin, P. & Huang, X. 2017. Revisit of rare earth element fractionation during chemical weathering and river sediment transport. *Geochemistry, Geophysics, Geosystems*, 18(3), 935–955. DOI: <https://doi.org/10.1002/2016gc006659>
- SUDELPA (Superintendência do Desenvolvimento do Litoral Paulista). 1987. *Plano Básico de desenvolvimento auto-sustentado para a região lagunar de Iguape e Cananéia*. São Paulo: Superintendência do Desenvolvimento do Litoral Paulista.
- Suguo, K., Tessler, M. G., Furtado, V. V., Esteves, C. A. & Souza, L. A. P. 1987. Perfilagens geofísicas e sedimentação na área submersa entre Cananéia e Barra de Cananéia. In: *Simpósio sobre ecossistemas da Costa Sul e Sudeste Brasileira* (pp. 234–241). São Paulo: Academia de Ciências do estado de São Paulo.
- Tessler, M. G. 1988. *Dinâmica sedimentar quaternária no litoral sul paulista* (phdthesis). Instituto de Geociências, Universidade de São Paulo, São Paulo.
- Tessler, M. G. & Furtado, V. V. 1983. Dinâmica de sedimentação das feições de assoreamento da região lagunar Cananéia-Iguape, Estado de São Paulo. *Boletim Do Instituto Oceanográfico*, 32(2), 117–124. DOI: <https://doi.org/10.1590/s0373-55241983000200002>
- Tessler, M. G. & Souza, L. A. P. de. 1998. Dinâmica sedimentar e feições sedimentares identificadas na superfície de fundo do sistema Cananéia-Iguape, SP. *Revista Brasileira de Oceanografia*, 46(1), 69–83. DOI: <https://doi.org/10.1590/s1413-77391998000100006>
- Tramonte, K., Figueira, R., De Lima Ferreira, P., Ribeiro, A., Batista, M. & De Mahiques, M. 2016. Environmental

- availability of potentially toxic elements in estuarine sediments of the Cananéia-Iguape coastal system, Southeastern Brazil. *Marine Pollution Bulletin*, 103(1–2), 260–269. DOI: <https://doi.org/10.1016/j.marpolbul.2015.12.011>
- Tramonte, K., Figueira, R., Majer, A., De Lima Ferreira, P., Batista, M., Ribeiro, A. & De Mahiques, M. 2018. Geochemical behavior, environmental availability, and reconstruction of historical trends of Cu, Pb, and Zn in sediment cores of the Cananéia-Iguape coastal system, Southeastern Brazil. *Marine Pollution Bulletin*, 127, 1–9. DOI: <https://doi.org/10.1016/j.marpolbul.2017.11.016>
- Tranchida, G., Oliveri, E., Angelone, M., Bellanca, A., Censi, P., D'elia, M., Neri, R., Placenti, F., Sprovieri, M. & Mazzola, S. 2011. Distribution of rare earth elements in marine sediments from the Strait of Sicily (western Mediterranean Sea): Evidence of phosphogypsum waste contamination. *Marine Pollution Bulletin*, 62(1), 182–191. DOI: <https://doi.org/10.1016/j.marpolbul.2010.11.003>
- Um, I. kwon., Man, S. C., Bahk, J. J. & Song, Y. H. 2013. Discrimination of sediment provenance using rare earth elements in the Ulleung Basin, East/Japan Sea. *Marine Geology*, 346, 208–219. DOI: <https://doi.org/10.1016/j.margeo.2013.09.007>
- Veloso, H. P., Rangel-Filho, A. L. R. & Lima, J. C. A. 1991. *Classificação da vegetação brasileira, adaptada a um sistema universal*. Rio de Janeiro: IBGE.
- Vinnarasi, F., Srinivasamoorthy, K., Saravanan, K., Gopinath, S., Prakash, R., Ponnumani, G. & Babu, C. 2020. Rare earth elements geochemistry of groundwater from Shanmuganadhi, Tamilnadu, India: Chemical weathering implications using geochemical mass-balance calculations. *Geochemistry*, 80(4), 125668. DOI: <https://doi.org/10.1016/j.chemer.2020.125668>
- Weber, W. 1998. *Geologia e Geocronologia da Ilha do Cardoso, sudeste do Estado de São Paulo* (mathesis). Universidade de Sao Paulo, Agencia USP de Gestao da Informacao Academica (AGUIA), São Paulo. <https://doi.org/10.11606/d.44.1998.tde-14102015-155051>
- Wedepohl, K. H. 1995. The composition of the continental crust. *Geochimica et Cosmochimica Acta*, 59(7), 1217–1232. DOI: <https://doi.org/10.1180/minmag.1994.58a.2.234>
- Wu, K., Liu, S., Kandasamy, S., Jin, A., Lou, Z., Li, J., Wu, B., Wang, X., Abdrahim Mohamed, C. & Shi, X. 2019. Grain-size effect on rare earth elements in Pahang River and Kelantan River, Peninsular Malaysia: Implications for sediment provenance in the southern South China Sea. *Continental Shelf Research*, 189, 103977. DOI: <https://doi.org/10.1016/j.csr.2019.103977>
- Yang, S. Y., Jung, H. S., Choi, M. S. & Li, C. X. 2002. The rare earth element compositions of the Changjiang (Yangtze) and Huanghe (Yellow) river sediments. *Earth and Planetary Science Letters*, 201(2), 407–419. DOI: [https://doi.org/10.1016/s0012-821x\(02\)00715-x](https://doi.org/10.1016/s0012-821x(02)00715-x)
- Yusoff, Z., Ngwenya, B. & Parsons, I. 2013. Mobility and fractionation of REEs during deep weathering of geochemically contrasting granites in a tropical setting, Malaysia. *Chemical Geology*, 349–350, 71–86. DOI: <https://doi.org/10.1016/j.chemgeo.2013.04.016>